

AD-A100 827

AIR FORCE INST OF TECH WRIGHT-PATTERSON AFB OH SCHO0--ETC F/6 10/2
PRIME POWER TO PULSE CONDITIONING INTERFACE METHODS. (U)

DEC 80 J R SILVA
AFIT/GE/EE/80D-39

UNCLASSIFIED

NL

1 OF 1
AD A
100827

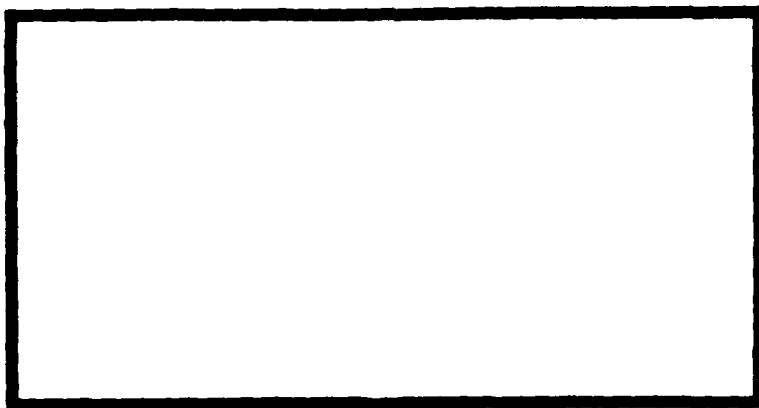
END
100827
7-31
DTIC

DDC

AD 2
200-200-
AD 2



0
LEVEL II



DTIC
ELECTED
JUL 1 1981
S D

UNITED STATES AIR FORCE
AIR UNIVERSITY
AIR FORCE INSTITUTE OF TECHNOLOGY
Wright-Patterson Air Force Base, Ohio

DISTRIBUTION STATEMENT A

Approved for public release:
Distribution Unlimited

81 6 30 032

DTIC FILE COPY

AFIT/GE/EE/80D-39

| | |
|-----------------|---|
| Accession For | X |
| NTIS GRA&I | |
| DTIC TAB | |
| Unlimited | |
| Justified (yes) | |
| By _____ | |
| Distribution: | |
| Aviation | |
| Aerospace | |
| Dist | |
| R | |

PRIME POWER TO PULSE CONDITIONING
INTERFACE METHODS
THESIS

AFIT/GE/EE/80D-39 Jaime R. Silva
2d LT USAF

Approved for public release; distribution unlimited.

AFIT/GE/EE/80D-39

PRIME POWER TO PULSE CONDITIONING
INTERFACE METHODS

THESIS

Presented to the Faculty of the School of Engineering
of the Air Force Institute of Technology
Air Training Command
in Partial Fulfillment of the
Requirements for the Degree of
Master of Science

by

Jaime R. Silva, B.S.
2d LT USAF
Graduate Electrical Engineering
December 1980

Preface

This thesis project was conducted not only as a part of the requirements for a masters program degree, but hopefully to make an immediate contribution to a current Air Force and Army joint program for the design of power supplies for future directed energy weapons.

I am most grateful to my professor and thesis advisor Captain Fred Brockhurst for his guidance during all phases of this thesis work. His willingness and ability to help me made possible this report.

The hardware tests were conducted at the Electrical Equipment Division U.S. Army Mobility Equipment Research and Development Command (MERADCOM), Fort Belvoir, Virginia. Since this was my first working experience, not much would have been done without the help and cooperation of the following people from MERADCOM.

I would like to express my gratitude to my advisors Dr. Alois L. Jokl and Dr. Larry I. Amstutz who gave me confidence and constant encouragement to carry on with this task. The test system was assembled by Mr. David Presley who assisted me during the experimental portion of the project. His knowledge and experience proved useful, especially when Murphy's law manifested itself, saving me much time and effort. Special acknowledgement is due to Mr. James Ferrick who provided constructive criticism and stimulating discussion on almost every aspect of this project.

Jaime R. Silva

Table of Contents

| | <u>Page</u> |
|---|-------------|
| Preface | ii |
| List of Figures | |
| List of Tables. | |
| Abstract | |
| I. Introduction | 1 |
| Background. | 1 |
| Problem | 1 |
| Scope | 2 |
| II. DC Resonant Charging | 3 |
| Theory - Introduction | 3 |
| Analysis of Voltage Sagging | 4 |
| Computer Programs | 6 |
| Effect of Voltage Sagging | 8 |
| Experimental Equipment & Instrumentation. . | 20 |
| Description of Pulser | 24 |
| Modifications Made to the Pulser. | 26 |
| Operation of Pulser | 27 |
| General Approach. | 27 |
| Results - Prime Power System. | 29 |
| Generator | 29 |
| Vibration & Heating | 29 |
| Voltage Regulator | 29 |
| Sag on Output Voltage | 32 |
| Pulser Performance. | 36 |
| Network Voltage & Charging Current. | 36 |
| Resonance Frequency | 38 |
| III. AC Resonant Charging | 40 |
| Theory - Introduction | 40 |
| Analysis | 40 |
| Experimental Equipment & Instrumentation. . | 42 |
| Description of Pulser | 44 |
| Operation of Pulser | 44 |
| Results - Resonance Frequency | 47 |
| IV. Conclusions & Recommendations. | 50 |
| Recommended Additional Work | 51 |
| DC Resonant Charging. | 51 |
| AC Resonant Charging. | 51 |

Table of Contents

| | <u>Page</u> |
|--|-------------|
| Bibliography | 52 |
| Appendix A: Mathematical Analysis of DC Resonant Charging. | A-53 |
| Appendix B: Computer Programs | B-56 |
| Appendix C: Additional Case | C-62 |
| Appendix D: Major Parts List. | D-64 |
| Vita | 65 |

List of Figures

| <u>Figure</u> | | <u>Page</u> |
|---------------|---|-------------|
| 1 | Equivalent DC Resonant Circuit | 4 |
| 2 | Plot of Average Input Power vs. Sag Constant . | 7 |
| 3 | Plot of Capacitor Voltage vs Time for 0% Sag . | 8 |
| 4 | Theoretical Plot of Maximum Capacitor Voltage vs Sag Constant. | 9 |
| 5 | Theoretical Plot of Resonance Frequency vs Sag Constant | 10 |
| 6 | Theoretical Plot of Average Power vs Sag Constant | 11 |
| 7 | Theoretical Plot of Peak Charging Current vs Sag Constant | 12 |
| 8 | Theoretical plots of the Charging Current and Capacitor Voltage for 0% Sag on Input Voltage. | 15 |
| 9 | Theoretical Plots of the Charging Current and Capacitor Voltage for 10% Sag on Input Voltage | 16 |
| 10 | Theoretical Plots of Charging Current and Capacitor Voltage for 15% Sag on Input Voltage | 17 |
| 11 | Theoretical Plots of the Charging Current and the Capacitor Voltage for 30% Sag on Input Voltage. | 18 |
| 12 | Theoretical Plots of the Charging Current and the Capacitor Voltage for 45% Sag on input Voltage. | 19 |
| 13 | Block diagram of DC Resonant Charging System . | 20 |
| 14 | DC Resonant Circuit. | 21 |
| 15 | Test Circuit Showing the Test Points | 22 |
| 16 | Schematic of Generator Instrumentation | 25 |
| 17 | Schematic Diagram of the DC Pulser | 25 |
| 18 | Scope Traces | 30 |
| 19 | Scope Traces | 31 |

| <u>Figure</u> | | <u>Page</u> |
|---------------|--|-------------|
| 20 | Scope Traces | 52 |
| 21 | Scope Traces | 55 |
| 22 | Scope Traces | 55 |
| 23 | Scope Traces | 54 |
| 24 | Scope Traces | 55 |
| 25 | Scope Traces | 57 |
| 26 | AC Charging Circuit. | 57 |
| 27 | Block Diagram of AC Resonant Charging System | 42 |
| 28 | AC Resonant Circuit. | 43 |
| 29 | Schematic Diagram of AC Pulser | 45 |
| 30 | Scope Traces | 48 |
| A-1 | Plot of Eq(1) for Two Charging Cycles . . | A-53 |
| B-1 | Fortran Program for Varying Sag Constant . | B-58 |
| B-2a | Fortran Program for Charging Current and Capacitor Voltage Waveforms (Sheet 1 of 2) | B-59 |
| B-2b | Fortran Program for Charging Current and Capacitor Voltage Waveforms (Sheet 2 of 2) | B-60 |
| C-1 | Scope Trace of DC Bus Voltage (TOP) and Charging Current (5 KV/div, 2A/div). . . . | C-62 |
| C-2 | Scope Trace of DC Bus Voltage (TOP) and Capacitor Voltage (5 KV/div) | C-65 |

List of Tables

| <u>Table</u> | | <u>Page</u> |
|--------------|---|-------------|
| 1 | Example of Pulser Performance for 0% and 48% Sag | 13 |
| 2 | Comparison of Calculated Values vs Actual Values. | 39 |

Abstract

"AC and DC resonant charging hardware tests were conducted with a 15KW DOD standard 400 Hz generator as prime power. DC resonant charging caused vibrations of the generator at the pulsing frequency and instability of the voltage regulator due to the very irregular generator voltage waveform. The input DC voltage to the pulser sagged causing the performance to be lower than expected. An analysis of this problem and the theory to account for this sag is presented.

Problems with the triggering of AC resonant charging were not solved in time for this report. The experimental set up of AC resonant charging is presented. AC resonant charging caused no negative impact on the generator which is a great advantage over DC resonant charging.

I. Introduction

Background

This project is a study of the interface between prime power systems and pulse conditioning systems for the use in electrical power generation for future directed energy systems.

The Army and the Air Force are sponsoring university work for the development of computerized theoretical predictions. The results of this thesis investigation will be used to refine and validate computer predictions which may then be used by Army and Air Force scientists as design aids for the power supplies required in directed energy systems.

The pulser used for these tests was constructed by Army's ERADCOM and contained separate sections for AC and DC resonant charging.

Each section contained the resonant circuit, support equipment, and controls.

Problem

There are several approaches to the interface between prime power generating equipment and pulse conditioning equipment. This is a study of two design approaches, these are DC resonant charging and AC resonant charging.

General areas to be observed are the impact on the prime power equipment of the charging scheme used and the performance of the charging method with this particular

kind of prime power source. Attention is given to grounding methods, electro-magnetic phenomena, physical layout of the components, and control requirements.

Scope

A laboratory set up was assembled using a 10kW ac standard 400HZ generator to try out each of the charging methods. These set ups included appropriate controls. Each system was instrumented so actual performance could be compared with present theory.

A mathematical analysis was done for the DC resonant charging method and the resulting equations were used in two computer program. These computer programs provided the theoretical solutions to which observed performance was compared.

The AC resonant charging theory is discussed and the experimental set up described. No data was collected for AC resonant charging since problems with the triggering logic were not solved in time for this report. Several observations on AC resonant charging are included.

II. DC Resonant Charging

Theory

Introduction

The theory of DC resonant charging circuits has long been developed and circuits of this kind used for many years. The problem studied here was the effect of DC resonant charging on the prime power equipment of a possible power supply for directed energy weapons. The prime power source was a three phase system composed of a generator, a transformer, and a full wave bridge rectifier.

When a generator has a rectified load its voltage waveform is deformed by the commutation of the current on the rectifiers. In this case the load is also varying as a series of half sines and to make matters worse the discharge pulsing is reflected back on the generator waveform. This irregular current waveform causes additional heat losses in the generator windings and throughout the prime power system. The generator also vibrates at the pulsing frequency, this is so because the torque is proportional to the load current.

The output voltage from the prime power system was observed to drop proportional to the load current, or sag, during each charging cycle. A mathematical approximation of this characteristic was done and a complete analysis of its effect on the pulser performance was made.

This analysis is presented next, then theoretical results obtained from two computer programs are presented. These computer programs were developed using the equations obtained from the mathematical analysis.

Analysis of Voltage Sagging

The sagging on the output voltage during one charging cycle is determined by the generator and transformer reactance and the load current. The voltage regulator does not respond fast enough in that time period to make any changes in the shape of this sag. It is not discussed here how to determine the magnitude of this voltage sagging for a given system. However, the effect of this sagging on the pulser performance is studied in depth.

A DC resonant charging circuit can be represented as in Figure 1 below.

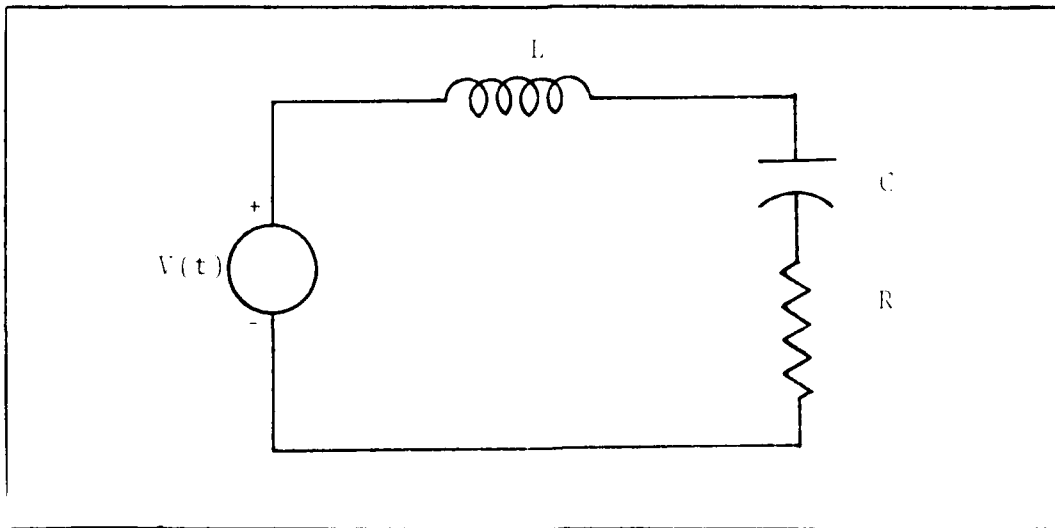


Figure 1 Equivalent DC Resonant Circuit

In Figure 1 L is the charging inductance, C is the total network capacitance and R is the sum of the charging inductor resistance and the equivalent load resistance.

The input voltage $V(t)$ was represented for this analysis as in Equation 1.

$$V(t) = E_{bb} (1 - K i_c(t)) \quad (1)$$

where E_{bb} is the peak input voltage, K is a constant, and $i_c(t)$ is the charging current as a function of time.

A mathematical analysis for the circuit of Figure 1 with an input voltage as given by Equation 1 is included in Appendix A. This analysis resulted in the following equations for the charging current and the capacitor voltage respectively.

$$\begin{aligned} i_c(t) &= \frac{E_{bb} - V_0}{WL} e^{-bt} \sin \omega t \\ &+ I_0 e^{-bt} (\cos \omega t - \frac{b}{\omega} \sin \omega t) \end{aligned} \quad (A-5)$$

$$\begin{aligned} V_c(t) &= E_{bb} + (E_{bb} - V_0) e^{-bt} (\cos \omega t + \frac{b}{\omega} \sin \omega t) \\ &+ \frac{I_0}{\omega C} e^{-bt} \sin \omega t \end{aligned} \quad (A-6)$$

where,

V_0 initial capacitor voltage

I_0 initial inductor current

$$b = \frac{R+K}{2L}$$

$$\omega = \frac{1}{LC} - b^2 = \text{circuit resonance frequency}$$

The pulser resonance repetition frequency is two times the circuit resonance frequency given above. From now on, every time resonance frequency is mentioned it is referring to the pulser frequency.

Equations (A-5) and (A-6), and other equations derived in Appendix A were used to develop two interactive fortran programs to calculate the theoretical results.

Computer Programs

Two computer programs were developed as an aid in producing theoretical results. These were also used to test the effects of changes in the system parameters. Appendix B contains a copy of each program and a brief description of how they work.

The first program calculated the peak voltage in the capacitor, peak charging current, resonance frequency, and average power for increasing values of input voltage sag. This was calculated for a given circuit and voltage level. This data was used as input to a plotting routine and plots of the mentioned parameters versus the sag on the input voltage were obtained. An example of these plots is shown in Figure 2.

For example, the sag constant on the horizontal axis of Figure 2 is 0.2 for 20% saggging on the input voltage, 0.45 for 45%, and so on.

These plots were useful to indicate the difference in performance for different magnitudes of voltage sagging.

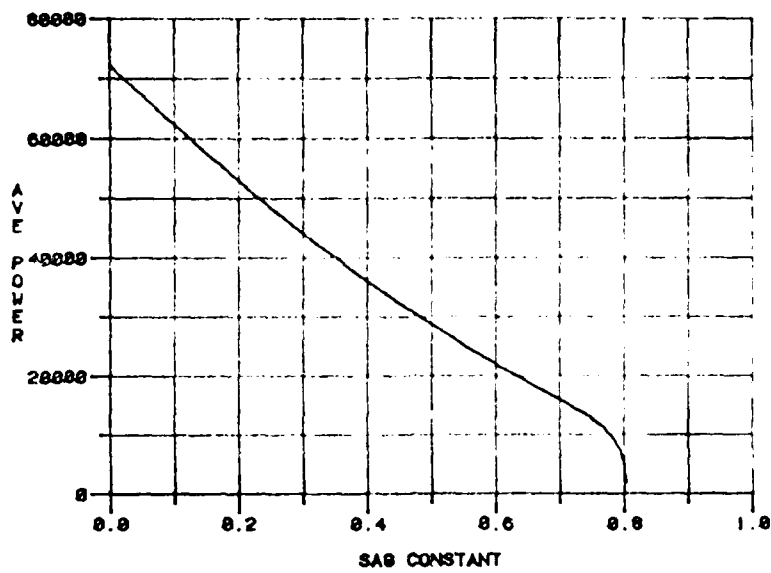


Figure 2 Plot of Average Input Power vs. Sag Constant

The second computer program used Equations (A-5) and (A-6) to generate a set of values for charging current and capacitor voltage versus time. The same plotting routine was then used to obtain the theoretical plots; these plots were used to compare to actual waveforms. Figure 3 on next page shows a plot obtained with this second program. The waveform shown is for the ideal case where the input voltage is a constant DC voltage.

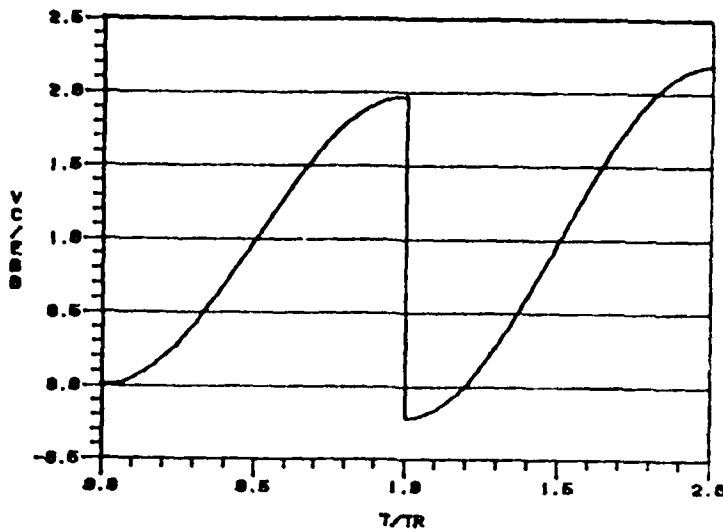


Figure 3 Plot of Capacitor Voltage vs. Time for 48% Sag

Effect of Voltage Sagging

For a constant input voltage the pulser would perform as predicted by Glasoe and Lebacqz (Ref 1, Chap 9). This case is shown in Figure 3 above. When the input voltage sags it is intuitive to say that the capacitor will charge to a lower voltage and that it will take a longer time to do so compared to the ideal case. In fact that is what happens in reality and the mathematical analysis reflects just that.

Figure 4 through 7 show how the maximum voltage in the capacitor, the resonance frequency, average power, and peak charging current will decrease as the magnitude of the sag increases. These plots are for a circuit with $L=2.9 \mu H$, $C=2.58 \mu F$, $R=17.5 \Omega$, $E_{ab}=10KV$, and $V_0 = -0.1 V_c(T_r)$. Results from Figures 4 through 7 for the ideal case and 48% sag are summarized in Table 1 on page 13.

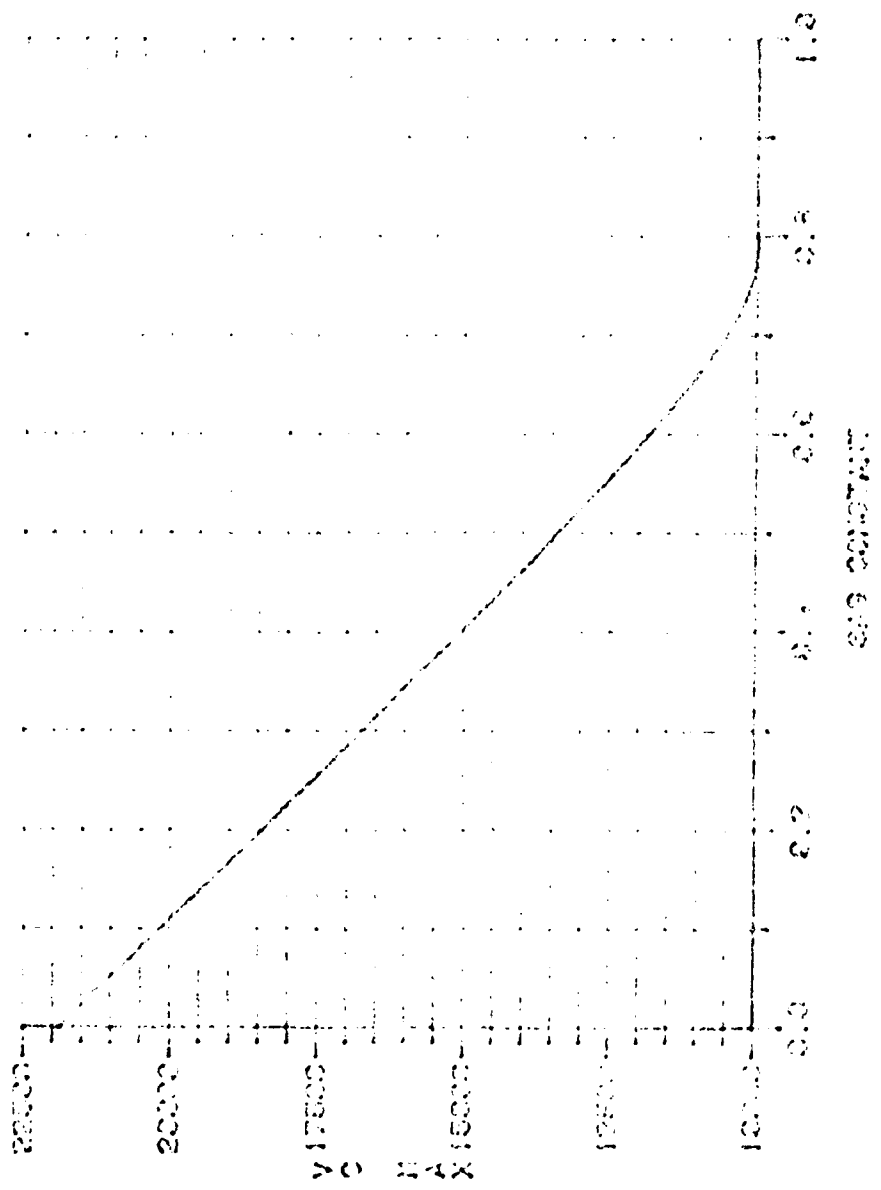


Figure 4 Theoretical Plot of Maximum Capacitor Voltage vs. Sag Constant

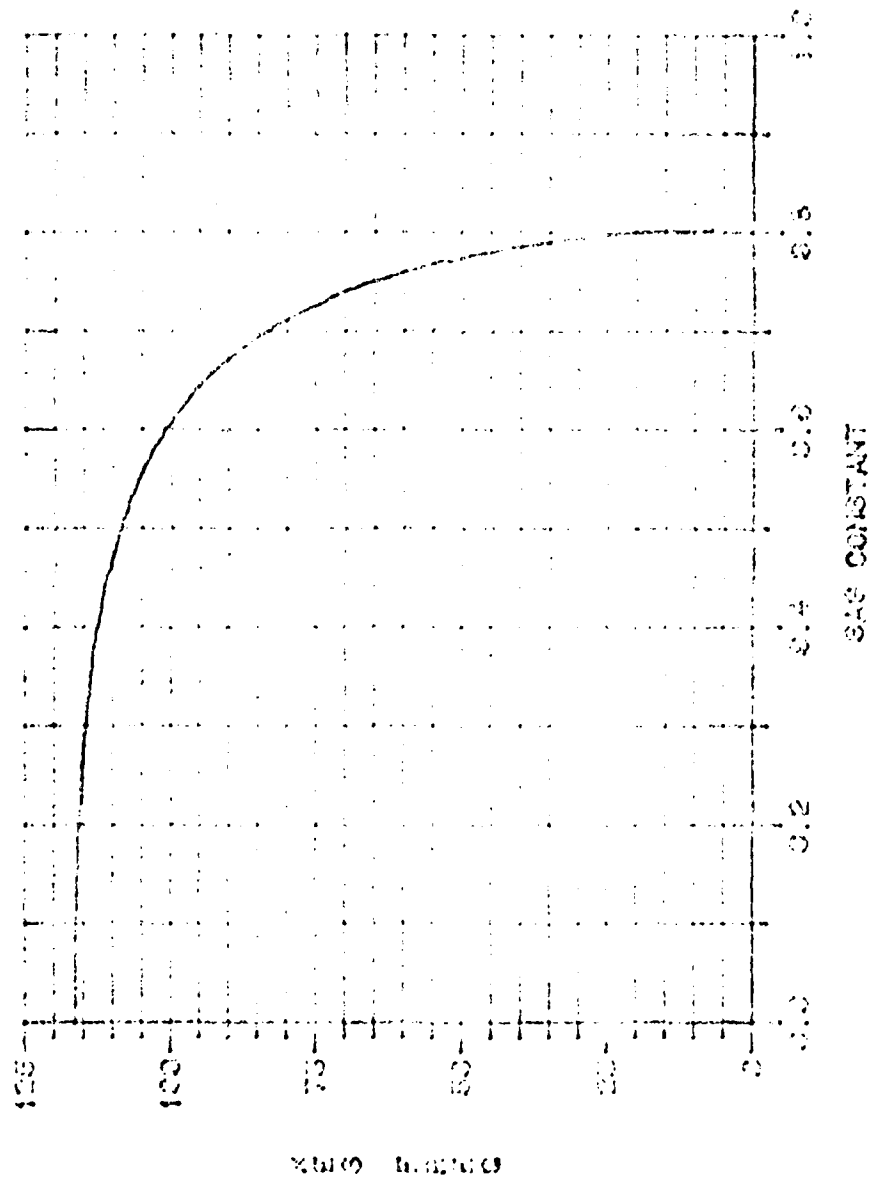


Figure 5 Theoretical Plot of Resonance Frequency
vs. Sag Constant

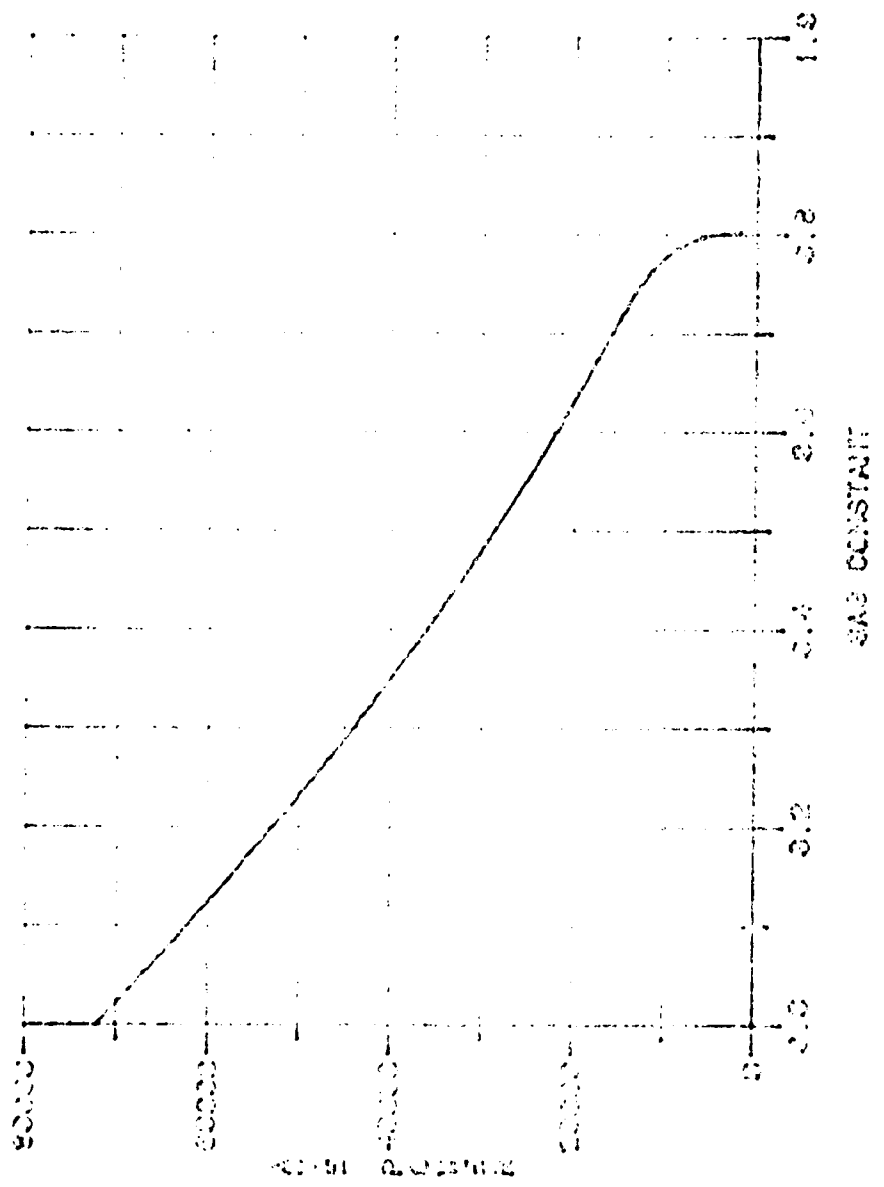


Figure 6 Theoretical Plot of Average Power vs.
Sag Constant

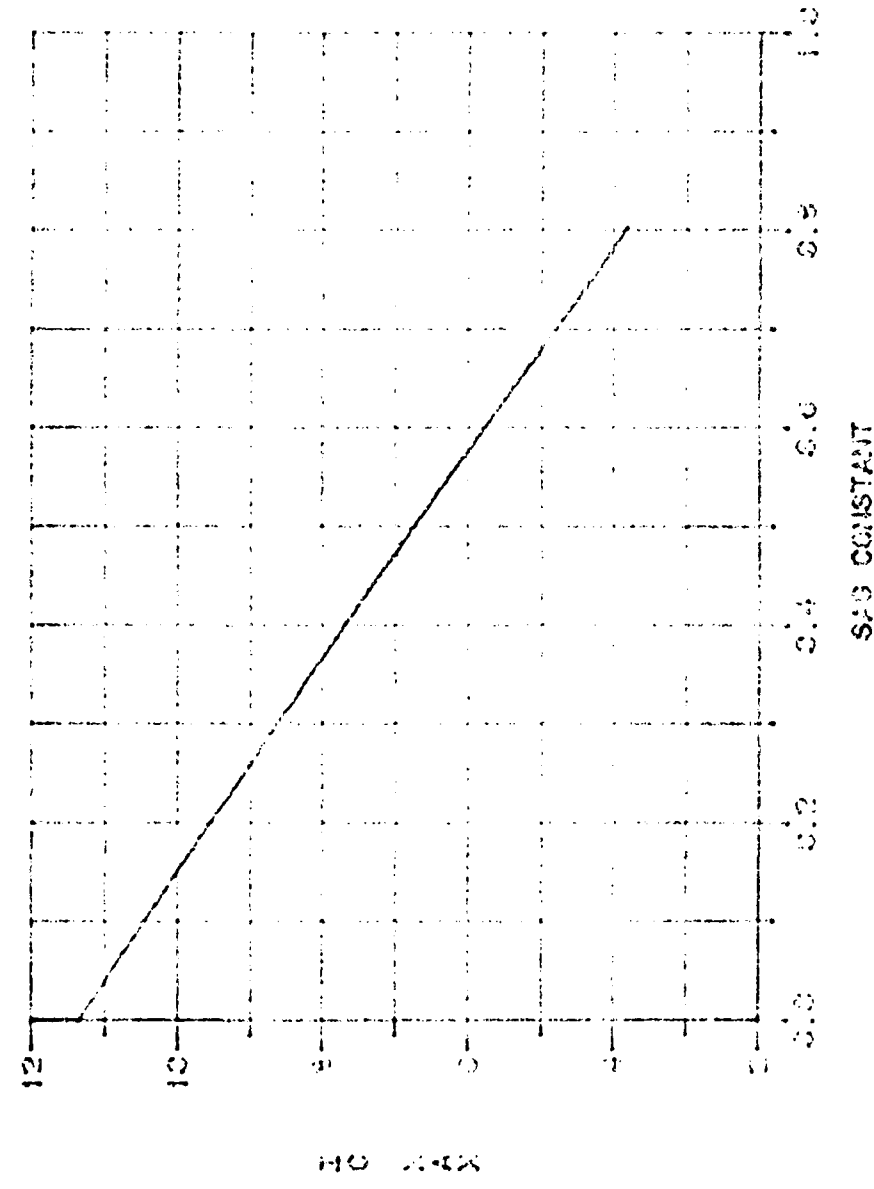


Figure 7 Theoretical Plot of Peak Charging Current vs. Sag Constant

Table 1 Example of Pulser Performance for Sag Constant of 0.0 and 0.48

| % SAG | W | $V_c(T_r)$ | P_{av} | I_{cp} |
|-------|-------|------------|----------|----------|
| 0 | 116.4 | 21.90 KV | 72.2 KW | 11.4 A |
| 48 | 109.6 | 13.75 KV | 30.0 KW | 6.9 A |

From this example and the theoretical graphs it can be seen that the biggest impact of the voltage sag is on the average power of the system.

The energy stored in the capacitor network per cycle is given by Equation 2.

$$E_s = \frac{1}{2} C [V_c(T_r)^2 - V_o^2] \quad (2)$$

Equation 3 below gives the energy input from the power supply per cycle.

$$E_I = V_{av} I_{av} T_r \quad (3)$$

Where V_{av} and I_{av} are the average input voltage and current respectively and T_r is the repetition period.

The average of the input voltage given by Equation 1 is

$$V_{av} = E_{bb} (1 - K I_{av}) \quad (4)$$

and the average input current is (Ref 1:362).

$$I_{av} = f_r C [V_c(T_r) - V_o] \quad (5)$$

where f_r is the repetition frequency or $f_r = \frac{1}{T_r}$.

The efficiency of DC charging is given by the ratio of the energy stored in the network in one cycle to the input energy from the power supply during that cycle.

Dividing Equation 2 by Equation 5, substituting the expression of I_{av} given by Equation 5, and simplifying we get the following expression for the efficiency.

$$\eta_C = \frac{V_C(T_r) + V_0}{2 V_{av}} \quad (6)$$

Using equations 4 through 6 the efficiency for the ideal case of Table 1 is 98.6% and for the other case it is 88.1%. Therefore the efficiency is reduced, which is another undesirable effect of the voltage sag.

Figures 8 through 12 show the current and voltage waveforms for the same circuit parameters. These are plotted for sag constant equivalent to 3, 10, 15, 30, and 45 percent sags respectively. The first cycle on each plot is for zero initial voltage and the second cycle is for an initial voltage $V_0 = 0.1 V_C(T_r)$.

From the plots on the following pages we note that the shape of the charging current changes and the peak to average current increases for a larger sag on the input voltage. This increases the heat losses throughout the circuit. Note also that the capacitor will charge to a smaller voltage. It is important to recognize that T_r is different for each case and increases with increasing sag.

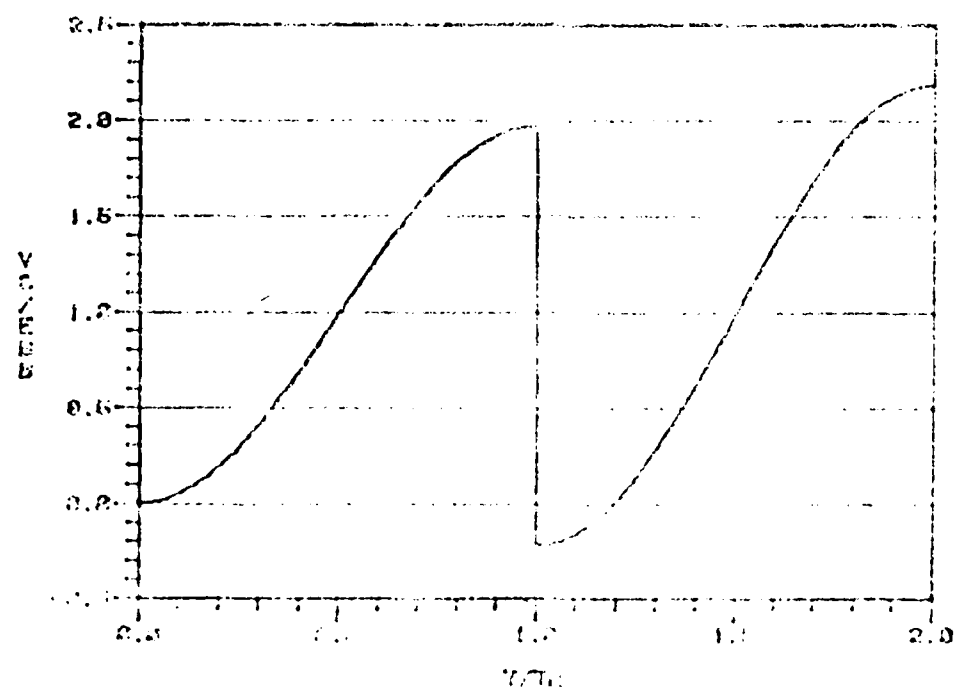
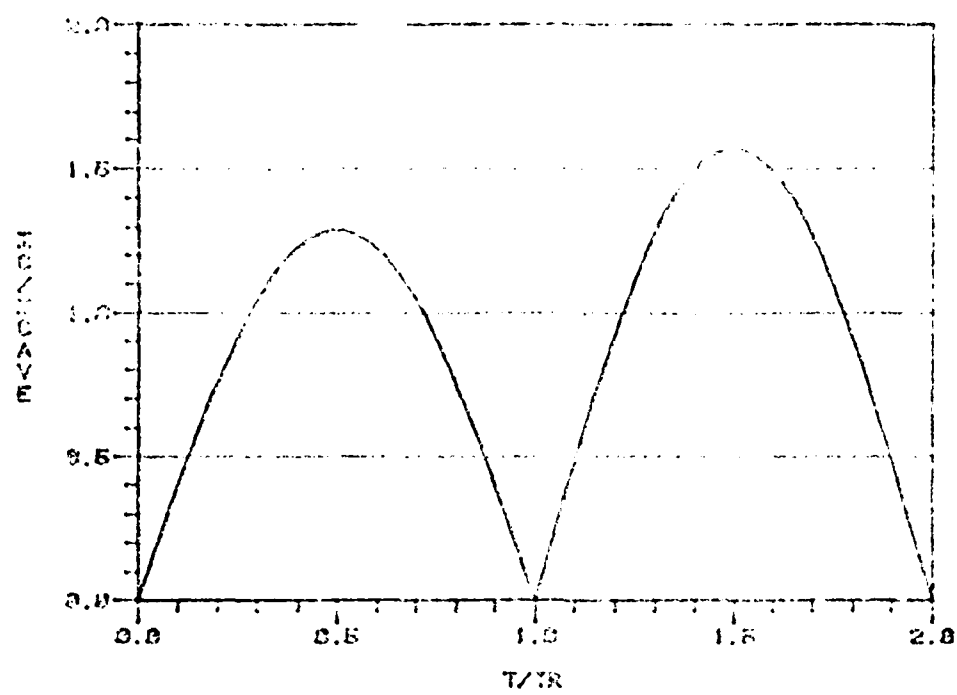


Figure 8. Theoretical Plots of the Charging Current and Capacitor Voltage for a Saw-on Input Voltage

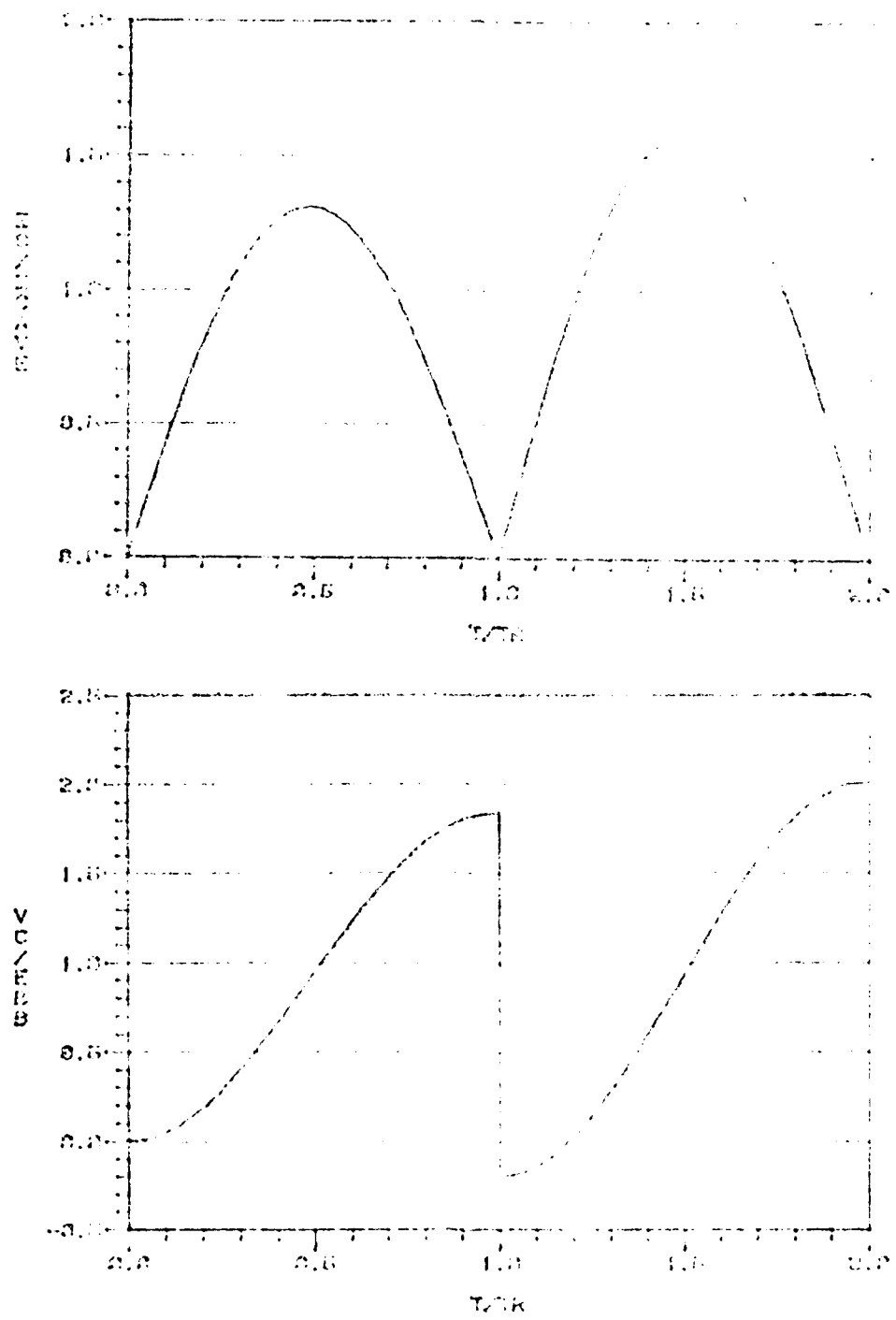


Figure 9. Theoretical Plots of the charging current and capacitor voltage for 10% sawtooth input voltage.

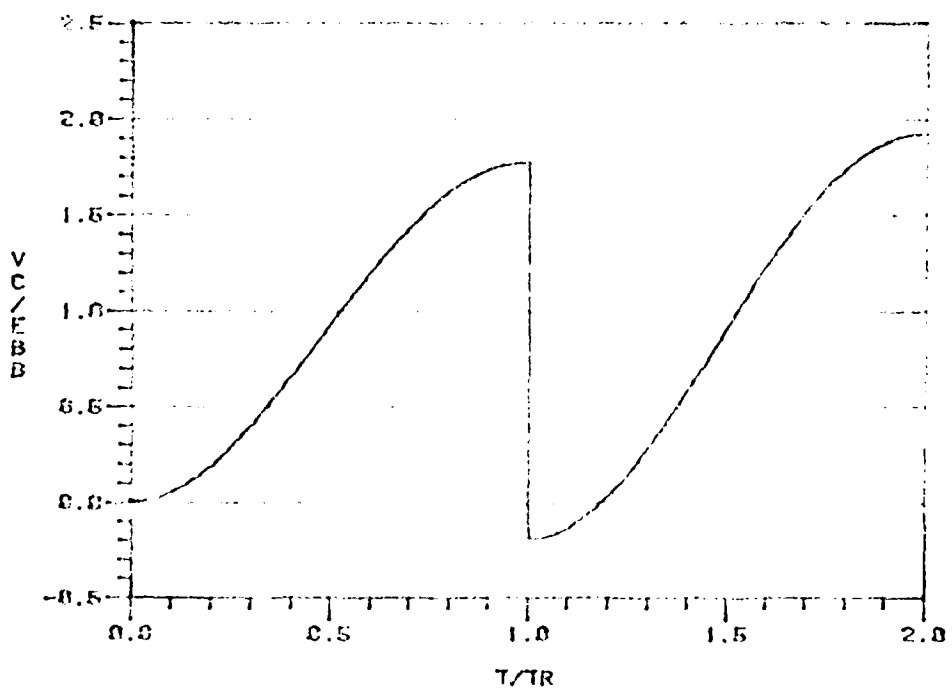
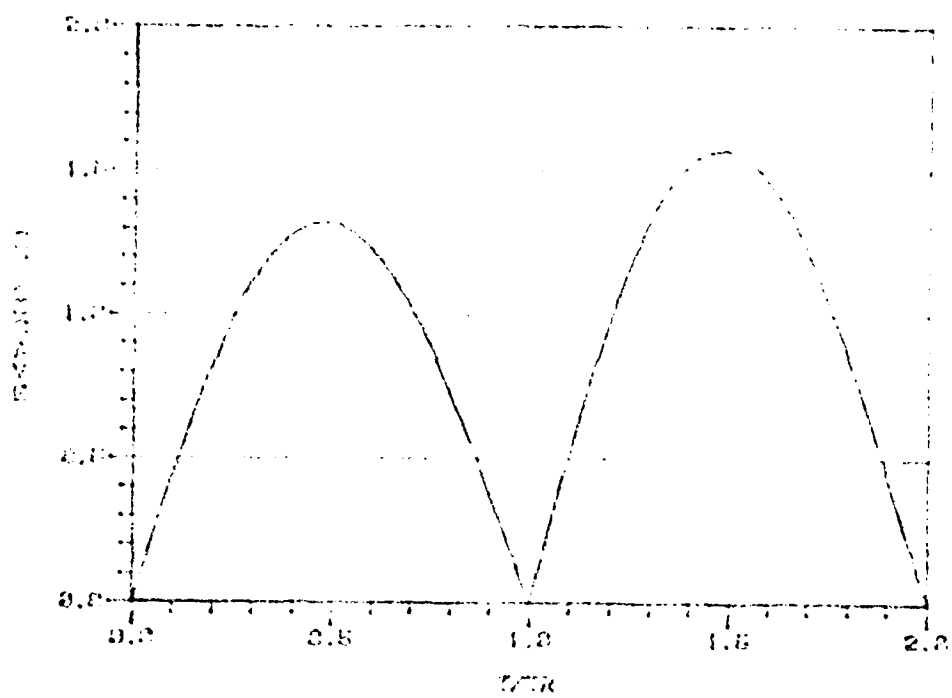


Figure 10 Theoretical Plots of the Charging Current and the Capacitor Voltage for 15% Sag on Input Voltage

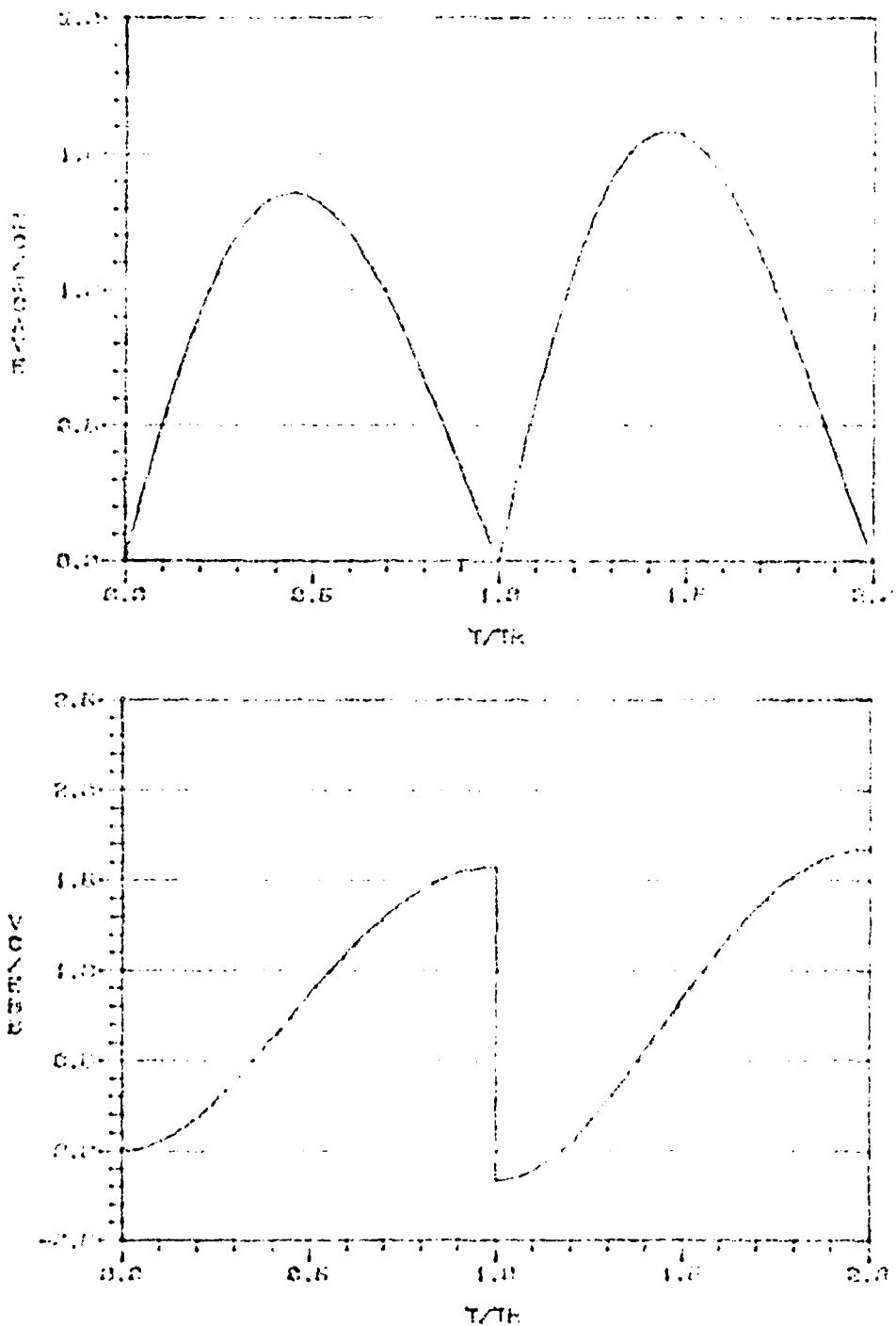


Figure 11 Theoretical Plots of the Charging Current and Capacitor Voltage for 30% Sag on Input Voltage

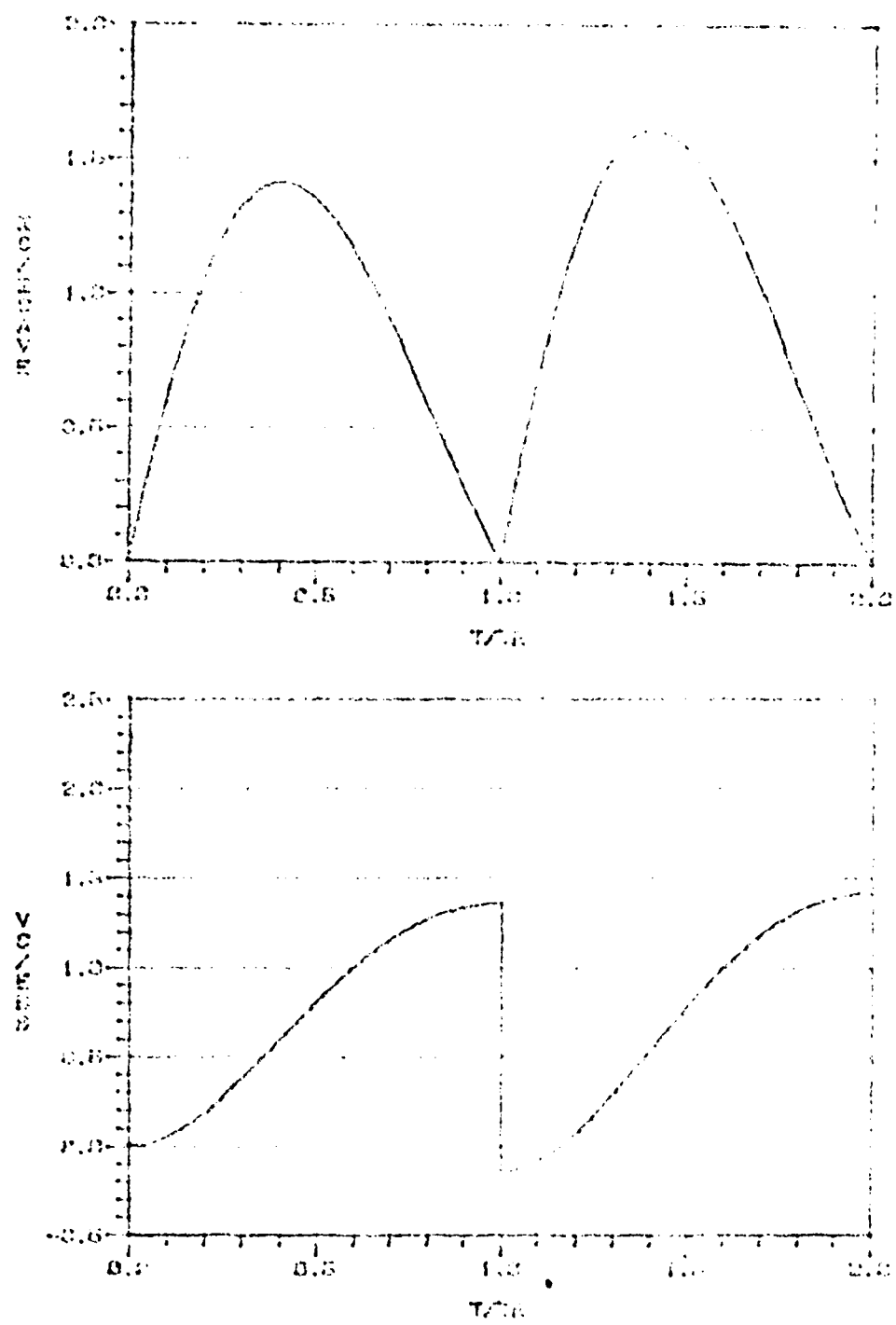


Figure 12 Theoretical Plots of the Charging Current and Capacitor Voltage for 45% Sag on Input Voltage

Experimental Equipment and Instrumentation

Figure 13 below is a block diagram of the experimental system.

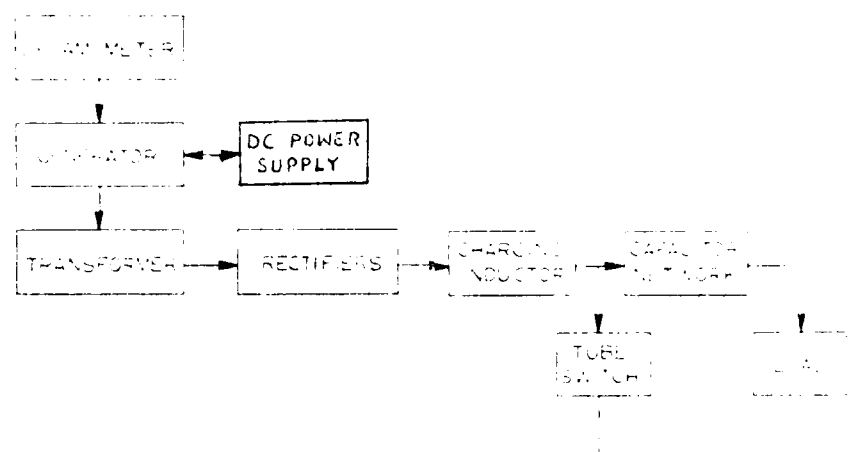


Figure 13 Block Diagram of DC Resonant Charging System

The prime mover was a 150 horsepower General Electric DC dynamometer. The generator was a DOD standard 15KW, 400HZ generator. A DC power supply was used for the generator exciter instead of a voltage regulator. The transformer had a voltage step-up ratio of 11:1. The liquid cooled full-wave bridge rectifier assembly had a nominal current capacity of 3 amperes per leg and a peak reverse voltage of 64KV. The charging inductor, capacitor network, tube switches, and the load were connected in the circuit shown in Figure 14.

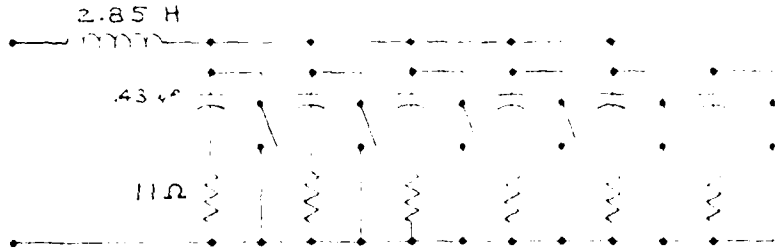


Figure 14 DC Resonant Circuit

Each of the six stages shown had a $0.43\mu\text{f}$ capacitor and an 11 ohm load resistor. The charging inductor was 2.85 Henrys. The tube switches were EG & G hydrogen thyratrons model HY-1A with a peak forward voltage of 20KV and a peak current of 0.5KA.

The schematic diagram of Figure 15 shows the test circuit with the test points marked a thru e.

The $0.0075\mu\text{f}$ capacitor was connected at the output of the full-wave bridge rectifier to protect the diodes from damage by a voltage spike.

Two high voltage contactors were used in the operation of the pulser. The line contactor K2 controlled the pulsing by opening or closing the DC bus into the pulser. The "dump"

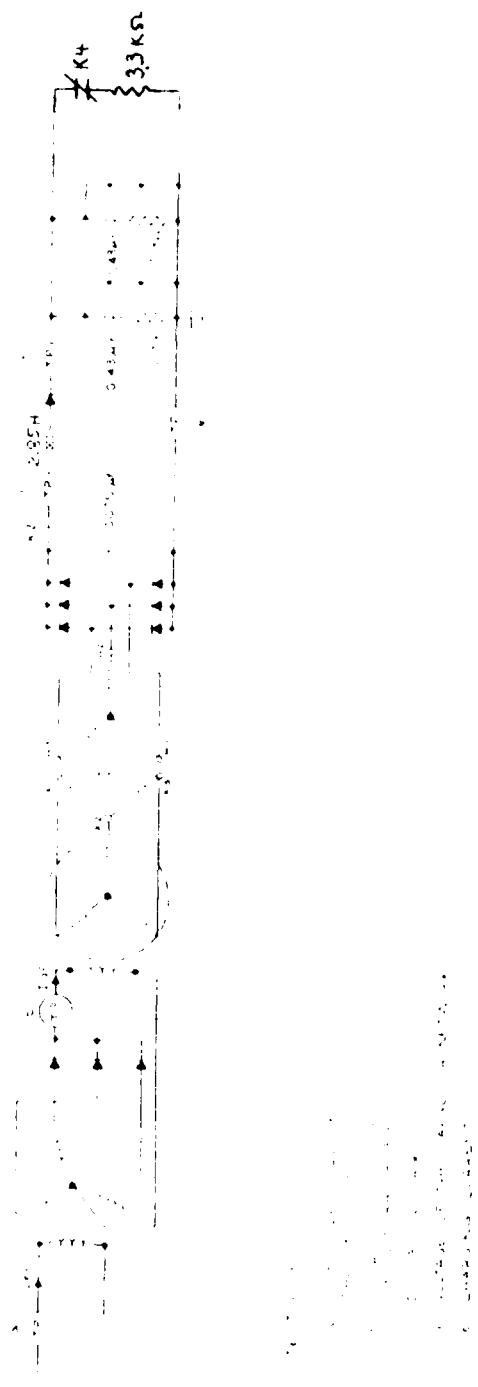


Figure 15 Test circuit Showing the Test points

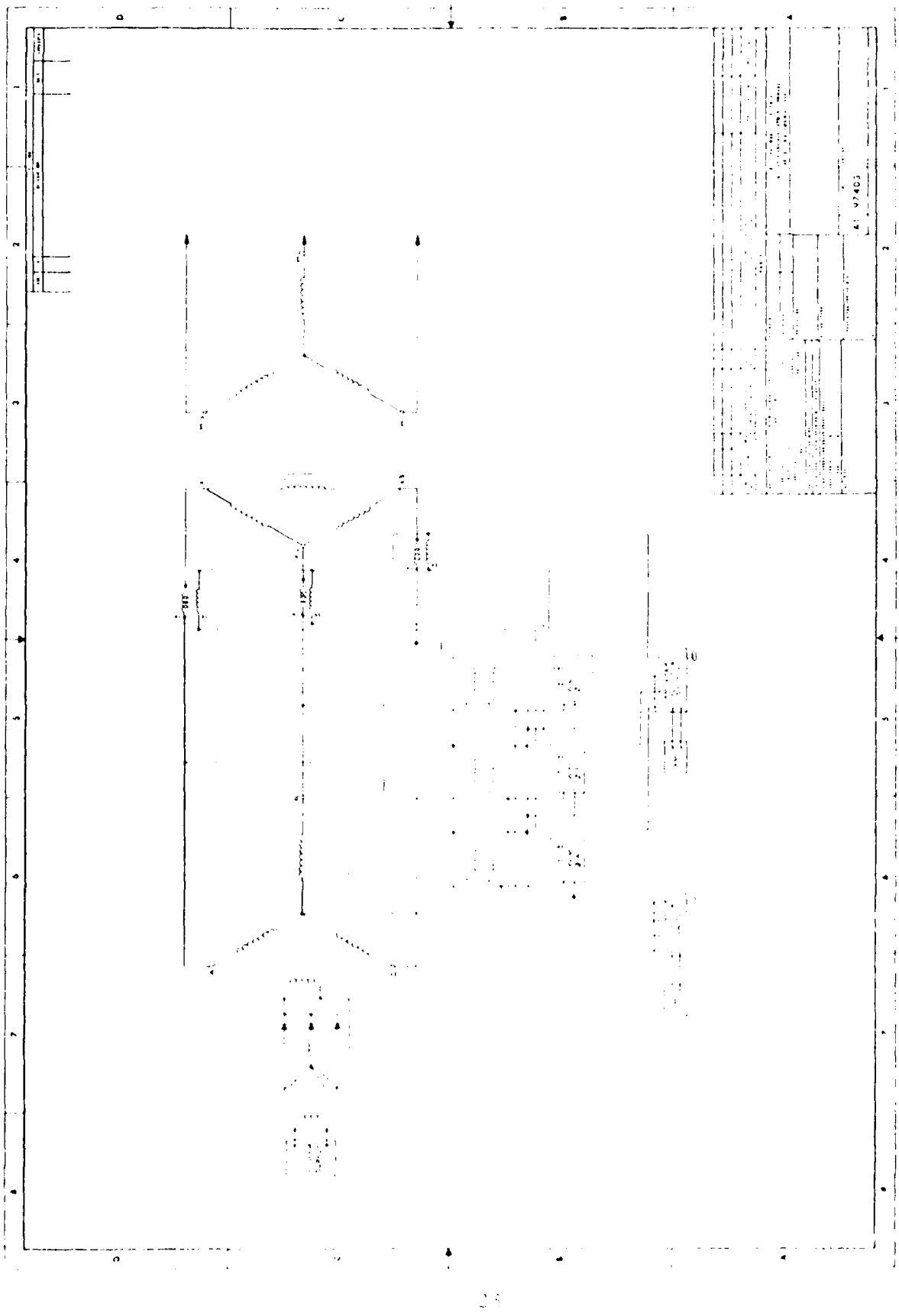


Figure 16 Schematic of generator instrumentation

contactor K4 closed after K2 opened so that any remaining voltage on the network was discharged thru a 3.3K resistor.

Note that a diode was connected between the charging inductor and the capacitor network. This is to prevent a current in the direction of the inductor when the pulser is discharged at a rate slower than resonance. Otherwise a high voltage spike is reflected back to the rectifiers and damage may occur.

The instrumentation diagram for the generator is shown in figure 16. This made it possible to read the average values of the phase voltage, current, and power delivered by the generator at all times.

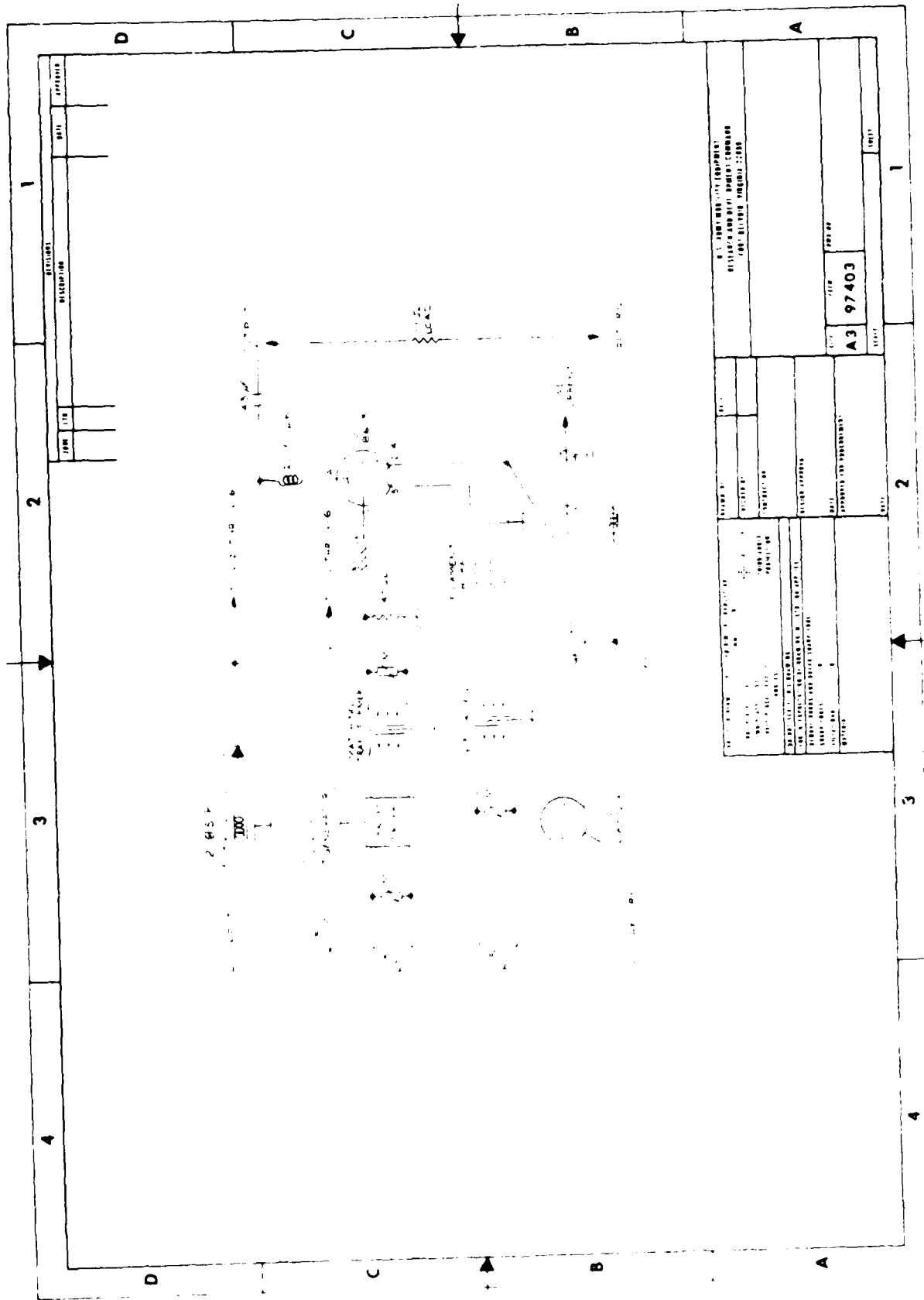
Description of Pulser

A schematic diagram of the pulser built by FRADOM is shown in figure 17.

A small inductance of approximately 20,henries series with the thyratrons was used to set the voltage in the capacitors to an initial negative value.

Metal oxide varistors (MOV) were used to suppress any high-voltage, high-frequency transients to vital components of the system.

The triggering circuit for the tubes consists of a function generator whose output is connected to the thyratron driver. The frequency of pulsing is set by the function generator. The output of the driver is connected through a matching transformer to a 140 ohm resistor and an MOV connected



in parallel. One output terminal of the transformer secondary is grounded to the chassis and from the other terminal a coaxial cable connects to a 300 Ω resistor on the grid of each tube. This arrangement proved to be susceptible to noise and led to false triggering of the thyratrons.

The heater circuit for the hot-cathode thyratrons is composed of a transformer and filament choke as shown in the schematic.

A big current transformer was used to monitor the load current and a 0.1 Ω resistor on the low voltage return with an ammeter was provided for average charging current readings.

Both the load return and the chassis were brought together to one point and grounded to the building ground.

Modifications Made to the Pulser

Electro-magnetic coupling, or transients conducted thru the electrical connections, were causing the tubes to pre-fire when the line contactor K2 was closed. A high voltage, high frequency voltage spike was observed in the grid of the false-triggered tube.

To prevent this some signal lines were re-routed away from high voltage lines and duplicate grounds were disconnected to eliminate any possible ground loop. This reduced the problem but did not eliminate it. Finally six MOVs were connected, one to each tube from grid to cathode and the false triggering was eliminated.

This proved the importance of the physical layout of

the components and the proper routing and shielding of electrical signal lines in this type of system.

Operation of Pulser

With the generator running at rated speed and the line contactor K2 open, excitation was applied to bring the DC voltage to the desired level. Then the "pulse" command was given. The dump contactor K3 opened, the line contactor K2 closed, and the pulser operated. At the command "stop", K2 opened and then K1 closed to discharge the energy left in the network. Pulsing frequency was adjusted with the function generator.

General Approach

The pulser was operated to collect data in the form of readings and photographs of oscilloscope traces.

When a disagreement between theoretical expectation and measured performance was found, an investigation into the cause was made. In each case either hardware malfunctions were corrected or additions or corrections to the theory were made.

The first part of this report presents the theory of DC resonant charging. A discussion of the different waveforms is followed by the results of the voltage test. The equipment and instrumentation are described and the results of the tests are presented.

The second part of the report presents the theory of AC resonant charging. The experimental set up is described and observations of the operation of this system are discussed. No data was collected on the AC resonant system since problems with the triggering circuit were not solved in time for this report.

RESULTS

Prime Power System

Generator

Figure 18 and 19 are photographs of the generator voltage and current, and the transformer secondary voltage and current (see Figure 15).

The ripple caused by the commutation of the current on the rectifiers is seen on all of these waveforms. One charging cycle has a duration of 9.1 msec compared to 2.5 msec for one generator cycle. So one charging cycle is almost four generator cycles. This can be clearly seen in Figure 18a where every four cycles the waveform of the current is repeated. These photographs correspond to 15kw output power from the generator.

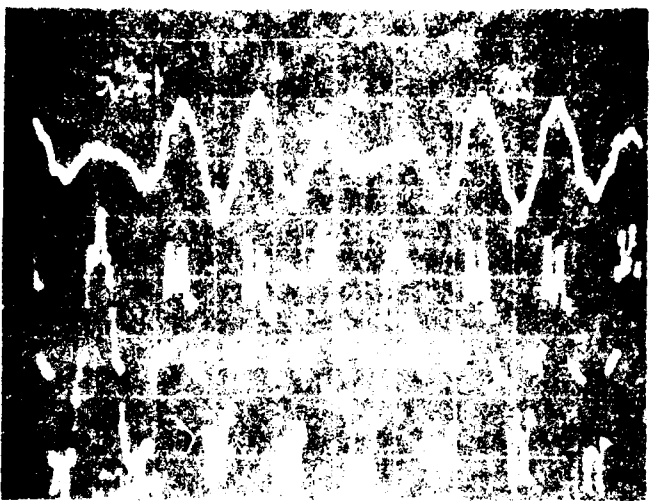
Vibration and Heating

The generator vibrated at the pulsing frequency. The torque pulsations were caused by the load current pulsing. Also because of the irregular generator voltage and current waveforms the generator heated faster since this caused increased losses on the windings.

Voltage Regulator

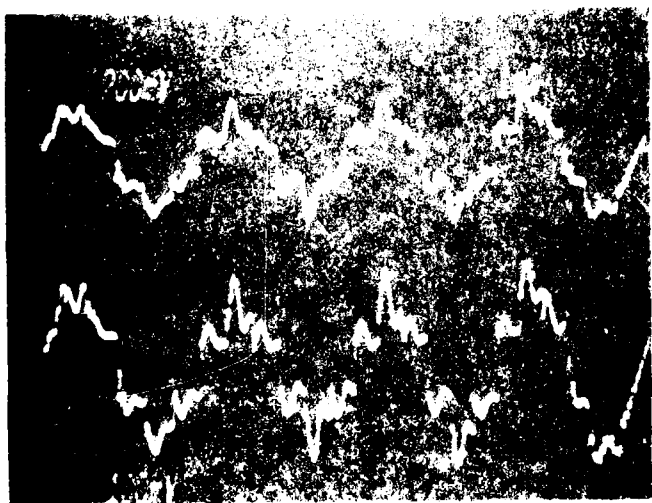
Figure 20 shows scope traces of the input voltage (top trace) and the capacitor network voltage (bottom trace).

The oscillations on both voltages were caused by the voltage regulator. As seen on the top trace the oscillations damp to a smaller magnitude but continue to about the



a) - tiene

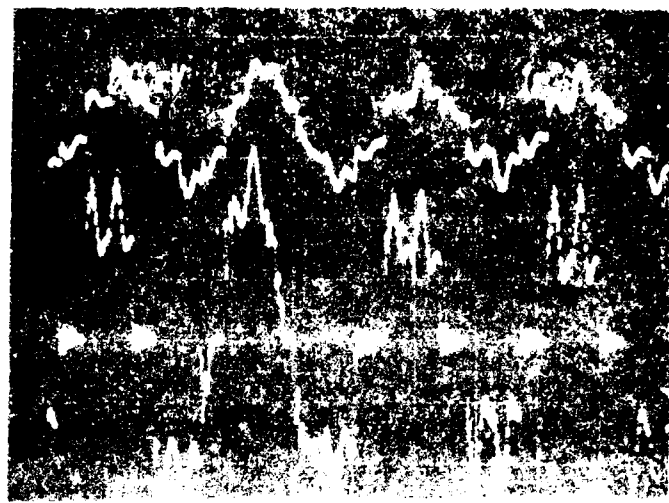
1°



b) - tiene

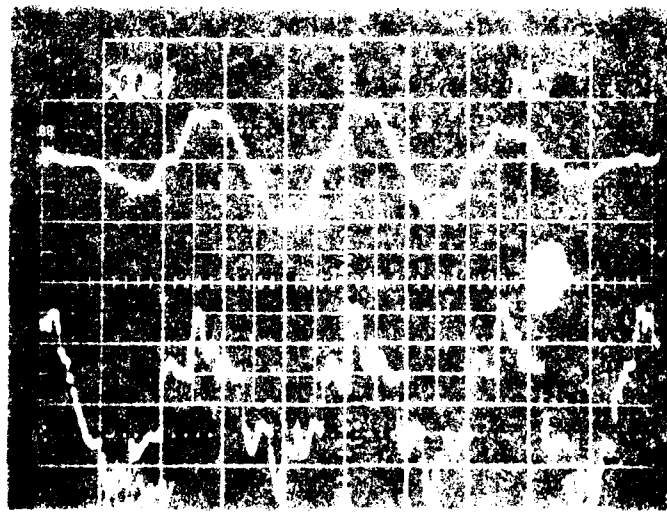
segundo

de la trayectoria
y el fondo)



d) Direct
Write

CF
Write



b) Trans
Print

CF
Write

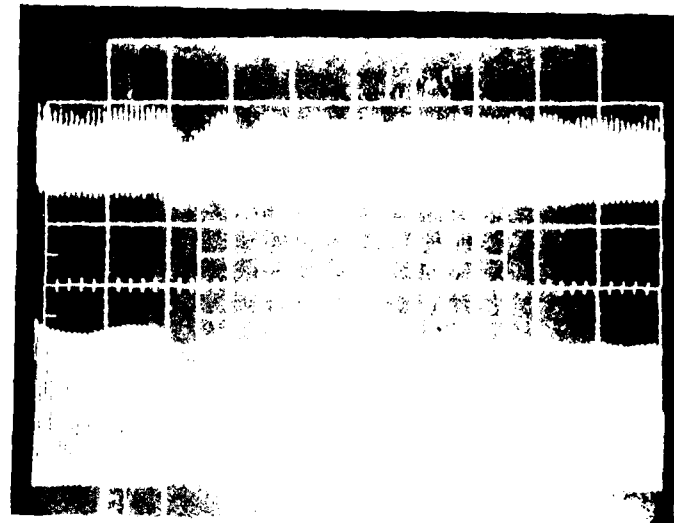


Figure 20 Scope Traces for the Pulser
(Test Points C and D respectively on Figure 15)

operation of the pulser. The reason for this malfunction was not investigated and a DC power supply was connected in place of the voltage regulator for the experiments.

Sag on Output Voltage

Figure 21 is a scope trace for the output voltage (top trace) and the inverted charging current (bottom trace). The output voltage sag follows the shape of the current very closely.

The frequency of the ripple on the output voltage is 2400HZ. Because of the big charging inductance the voltage will be equivalent to a DC voltage with a sinusoidal sag following the current waveshape. This criteria was used for the theoretical analysis.

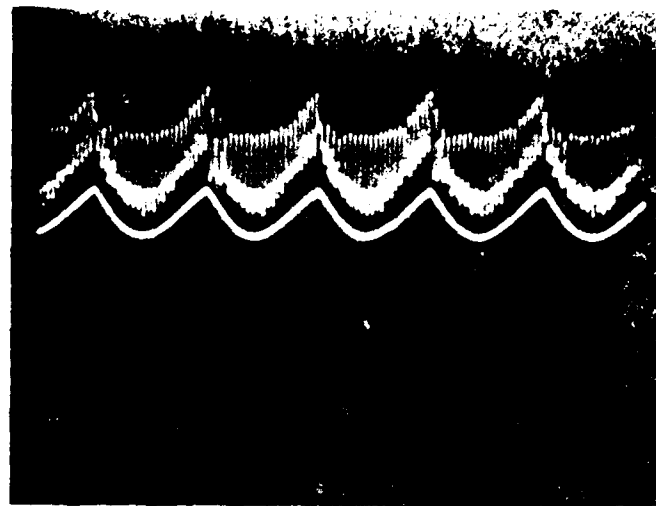


Figure 21. Wavy lines
in a dark field. (See also Figure 17 on page 17.)

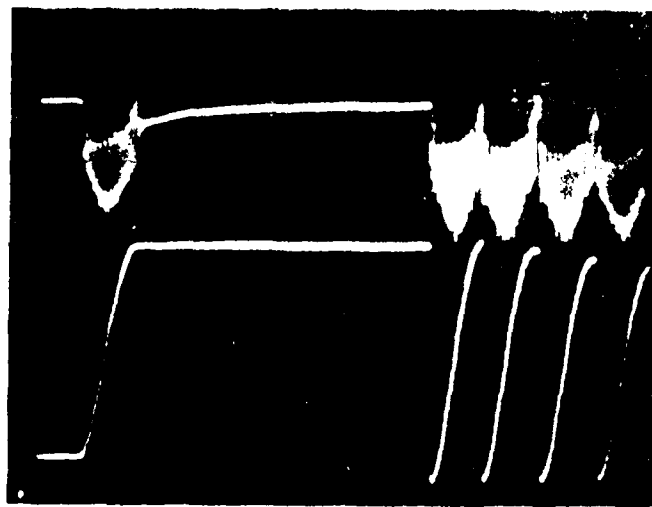


Figure 22. Wavy lines (continued).

but charged with generation droop factors. The plot shows the capacitor network voltage and its phase and amplitude voltage to the grid over four time intervals of 100 ms each.

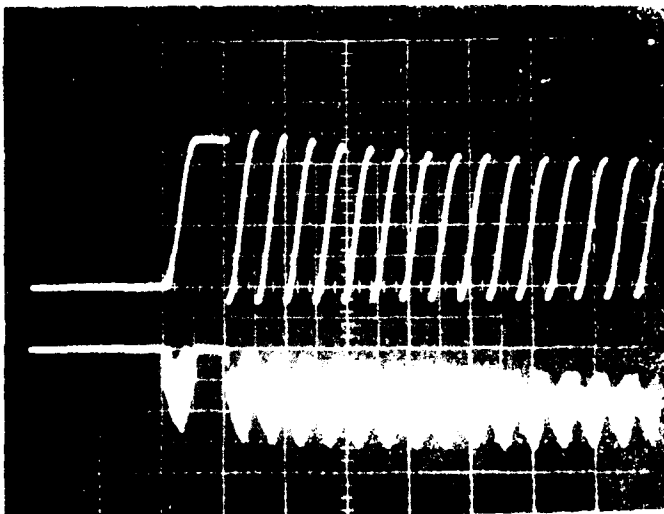
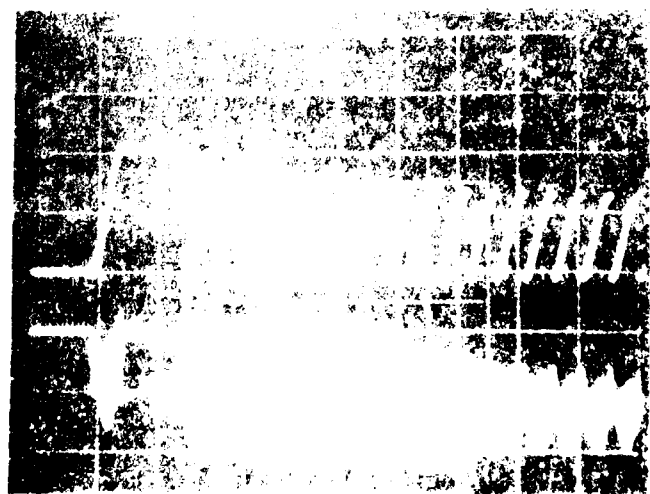
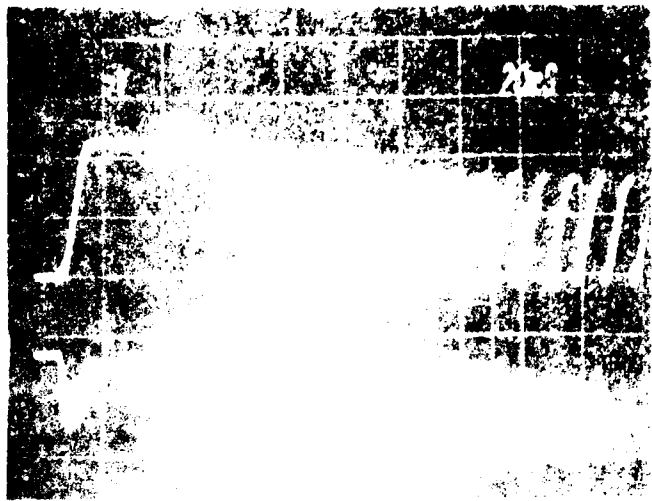


FIGURE 15. Scope Trajectories from the Initial Point to the Last Point of Each Path.



few pulses and then both voltages remain at a constant level. This is because the generator has constant output voltage and when the generator is loaded the average output voltage falls to a lower value. Another observation from the photographs is that the magnitude of the ripple on the bus voltage is smaller for 400 Hz than for the other two frequencies.

Pulser Performance

Before delivery to MERADCOM, where this investigation took place, the pulser was tested at TRAMCOM to see if it worked properly. The prime power for TRAMCOM came from a rectified high voltage power line with a bank of capacitors to provide a stiff DC voltage.

Resonance frequency was measured at 117 Hz and the peak voltage in the capacitors was 17KV for a DC input voltage of 8KV. This can be taken as the control test since the input was for all matters an infinite DC bus.

Network Voltage and Charging Current

Figure 25 shows the DC bus voltage, or input voltage, and the charging current for 29KW generator output power. By visual inspection of the scope traces of Figure 25 the following values were obtained for this case:

$$E_{pb} = 11.5 \text{ KV}$$

$$K_s = 0.50$$

$$I_{cp} = 6.6 \text{ A}$$

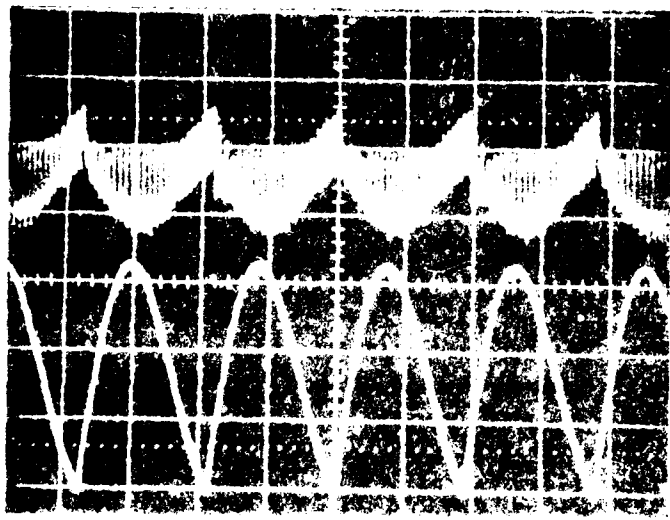


Figure 1.

am²

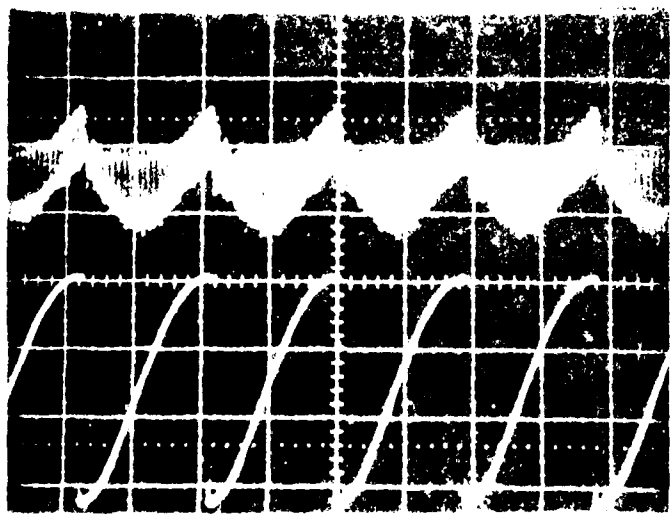


Figure 2.

am²

The resonance frequency was 106.6Hz and $P = 0.055$ for this system. The computer calculated value of $V_c(t_r)$ was 14.8KV. Figure 26 shows the DC bus voltage and capacitor voltage for this case. The actual value of the capacitor voltage was 15.0KV which is very close to the calculated value the theoretical peak charging current was 7.2 AMP and the average power was 35.0KW.

Resonance Frequency

The resonance frequency did not change with power level. A universal bridge was used to measure each of the six capacitors and the total capacitance was $2.58 \mu\text{f}$. The inductance was measured by applying a high voltage at 400 Hz and measuring voltage and current to obtain impedance. The inductance obtained by this method was 2.85 henrys and the resistance of the inductor was 6.5 ohms. These values for the circuit components yield a resonance frequency of 117.1 Hz for no sag. This is very close to 117 Hz measured at ERADCOM.

Table 2 below summarizes the actual and calculated values for two cases, third case is for no sag of the input voltage and is included for contrast.

Theoretical values were obtained with the first computer program. Another case is presented in Appendix C.

TABLE 2 Comparisons of Actual Values vs. Calculated Values

| E _{bb} | Calculated | | | | Measured | | | |
|-----------------|----------------------------------|-----------------|-----------------|----------------|----------------------------------|-----------------|-----------------|----------------|
| | V _c (T _r) | P _{av} | I _{cp} | f _r | V _c (T _r) | P _{av} | I _{cp} | f _r |
| 8KV | 10.5KV | 17kW | 5.0A | 108.3 | 9.6KV | 15kW | 4.0 | 106.6 |
| 11.5KV | 14.8KV | 35kW | 7.2A | 108.3 | 15.0KV | 29kW | 6.0 | 106.6 |
| 11.5KV | 24KV | 89kW | 12A | 117.4 | - | - | - | - |

III AC Resonant Charging

Theory

Introduction

AC resonant charging systems are less commonly used than DC resonant charging systems. There are many reasons for this, the concept of AC resonant charging is considerably more complicated and poses strict timing and control requirements. A major advantage of this interfacing method is that it does not introduce torque pulsations in the generator if the pulse repetition rate is low. If the generator voltage and current waveforms are smooth, the average power output can be controlled by varying the excitation field current (Ref. 117²).

As more studies are completed on AC resonant charging, the more attractive this interfacing method will be for pulsed power supplies (Ref. 2).

Analyse

An AC charging circuit can be represented as follows:

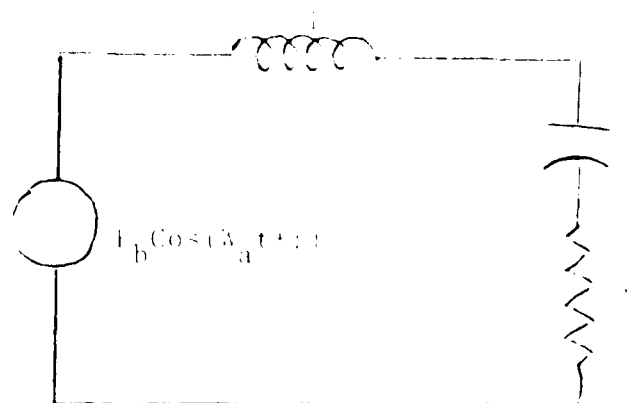


Figure 26 AC Charging Circuit

The equations for AC resonant charging are taken from reference 1 chapter 9,4,5. These equations are not presented here since they would not contribute to the scope of this discussion.

Half cycle AC resonant charging was used in this study. The circuit resonance frequency has to be equal to the alternator frequency, or

$$\omega = \omega_a$$

The condition for resonance is (Ref 1:385)

$$1 - LC\omega^2 = 0 \quad (8)$$

The voltage stepup ratio at the time of discharge is for half cycle charging (Ref 1:388)

$$\frac{V_c(\pi)}{E_b} = \frac{\pi}{2} \left(1 + \frac{\pi}{4Q}\right) \sin \phi + \frac{V_0}{E_b} \left(1 + \frac{\pi}{2Q}\right) \quad (9)$$

Where E_b is the peak AC input voltage, ϕ is the phase of the input voltage, V_0 is the initial capacitor voltage, and

$$Q = \frac{LW_a}{R} = \frac{1}{RC\omega_a} \quad (10)$$

Equation (9) is true for $\pi/2Q \ll 1$. For negligible losses Equation (9) becomes

$$\frac{V_c(\pi)}{E_b} = \frac{\pi}{2} \sin \phi + \frac{V_0}{E_b} \quad (11)$$

Equation (11) and other solutions in reference 1 indicate that for maximum efficiency ϕ has to be close to $\pi/2$. All this means is that charging should start at or near the beginning of a half cycle of the input voltage.

The difference between the resonance frequency of the individual circuits and the alternator frequency can be up to 10% without significant effect on the pulser operation (Ref 3). This is a great advantage given that a high power AC resonant system requires many resonant circuits that need to be tuned at the alternator frequency.

Experimental Equipment and Instrumentation

Figure 27 is a block diagram of the experimental system.

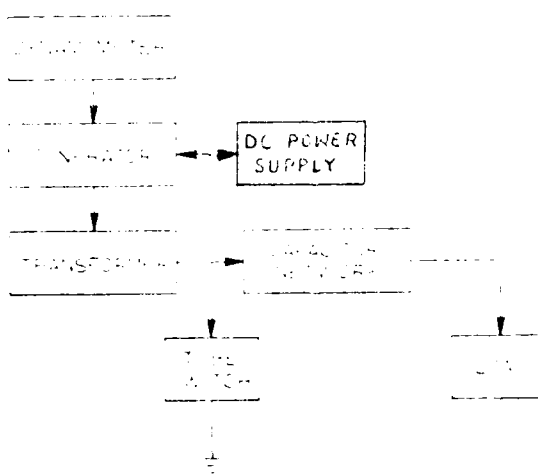


Figure 27 Block diagram of AC Resonant Charging System

The dynamometer, generator, and DC power supply were the same used for DC resonant charging. Three transformers with a voltage step-up ratio of 18.5:1 were connected in Y-Y configuration. These three high leakage transformers provided the total charging inductance. The AC resonant charging circuit is shown in Figure 28.

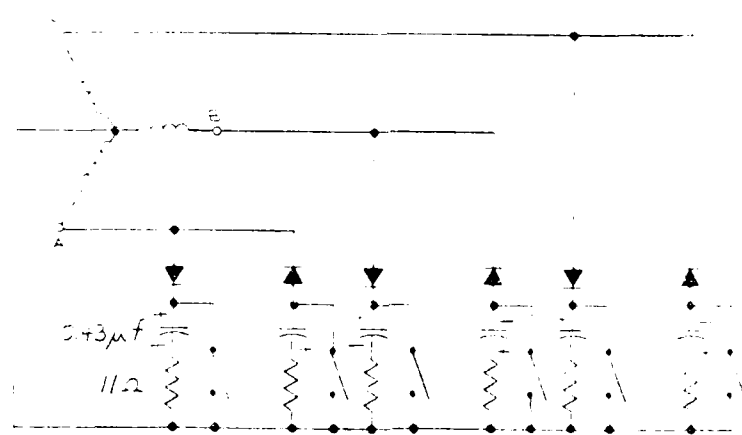


Figure 28 AC Resonant Circuit

This circuit has two $0.45\text{ }\mu\text{f}$. capacitors per stage, one for each half cycle of the phase voltage. The diodes were stacks with a total PRV of 30KV and a nominal current of 20 AMPS. The load for each of the six stages was an 11 ohm resistor. The tube switches were EG&G hydrogen thyratrons model HY-1A with a peak forward voltage of 70KV and a peak current of 0.5KA.

High voltage is preferred to low voltage at the same current voltage and capacity voltage.

Assumption of Fullness

¹ See, e.g., *U.S. v. Babbitt*, 100 F.3d 1250, 1254 (10th Cir. 1996) (“[T]he [Bald Eagle] Act does not prohibit the killing of bald eagles.”).

OPERATION OF THE C



FIGURE 1. Schematic diagram of the pulse

level for the sensing circuit, the logic box started triggering the thryatrons at the proper time. The output power of the pulser was regulated by controlling the exciter current.

Results

Resonance Frequency

The resonance frequency of one of the circuits is calculated next.

From Appendix D the leakage reactance of one transformer was 64.44 percent, or

$$z_L = \frac{64.44}{100} \cdot \frac{4440 \text{ V}}{47.5 \text{ A}} = 636 \text{ ohms}$$

The leakage inductance for 400 Hz was therefore

$$L_t = \frac{636}{2\pi(400) \text{ r/s}} = 0.253 \text{ HENRYS}$$

Also from Appendix D the alternator leakage reactance was 0.059 per unit, or

$$z_{La} = 0.059 \cdot \frac{240 \text{ V}}{26 \text{ A}} = 0.545 \text{ ohms.}$$

The transformer voltage ratio was 18.5 so at the secondary the alternator leakage inductance was

$$L_a = (18.5)^2 \cdot \frac{0.545}{2\pi(400) \text{ r/s}} = 0.074 \text{ HENRYS}$$

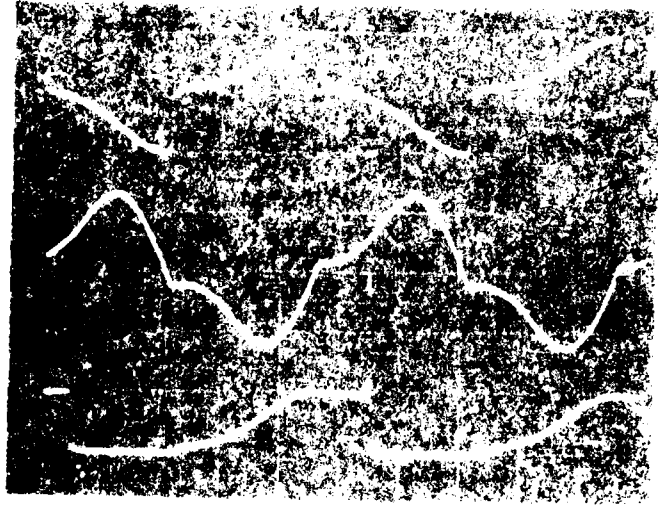
The total charging inductance was then

$$L_c = L_t + L_a = 0.327 \text{ HENRYS}$$

and the resonance frequency with C=0.45 μf

$$f = \frac{1}{2\pi\sqrt{0.45 \times 10^{-6} \cdot 0.327}} = 1.14 \text{ Hz}$$

which is very close to 400 Hz.



before entering the logic triggering box. Inside the logic box a zero crossing detector circuit and a timing circuit for each phase generated the triggering signals. The delay of the trigger pulse was set by adjusting the timers.

When the magnitude of the input voltage went above that shown in Figure 50 the triggering circuit generated multiple trigger signals per half cycle discharging the capacitors before they reached maximum voltage. This was a malfunction caused by the electronic logic circuit, this problem was not solved in time for this study.

Since the logic box worked only for very low voltage, and therefore low power, no data was collected on the system performance. General observations of this system are presented in the next chapter.

IV Conclusions and Recommendations

DC resonant charging is better known by people in the field of pulse power and is used more commonly than AC resonant charging. The problems presented by DC resonant charging on this study were vibration of the generator at the pulse repetition rate, irregular voltage and current waveforms in the generator, and lower performance of the DC resonant circuit due to input voltage sag. On the other hand, a DC resonant charging system is rather simple to construct and simple to trigger and control.

An AC resonant charging system has more hardware than an equivalent power DC resonant system and pulsing frequency is limited by the generator frequency. Also controls and triggering are far more complicated.

AC resonant charging does not cause a negative impact on the generator and this makes it very attractive.

Because of the high voltages and physical proximity of the components electromagnetic phenomena will cause problems for the signal lines. Proper shielding and routing of these lines together with transient suppressors (like MOV's, filter) have to be used.

The generator voltage control for DC resonant charging was a problem on the experiments and the alternative of feedforward voltage control should be considered. The sag of the DC bus voltage needs to be minimized for high performance and efficiency on a DC resonant charging system of this kind.

If this is done, DC resonant charging will be a satisfactory method for this kind of power supplies, except possibly for airborne power units.

More research on AC resonant charging is needed, especially on triggering schemes. AC resonant charging is without doubt a better interfacing method from the prime power system point of view.

Recommended Additional Work

DC Resonant Charging

Investigate the cause of instability of the voltage regulator and consider the approach of feedforward voltage control.

Define what system parameters, and how they do, determine the magnitude of the DC voltage sag. Suggest changes in the system to minimize this sag.

Install MILADOM controls and operate the system, make necessary changes to improve the system.

AC Resonant charging

Correct triggering circuit calibration. Study the effect of AC resonant charging on the generator. Study pulser performance and compare to theory.

Bibliography

1. Pulse Generators, G. N. Glasoe and J. V. Lebacqz; Radiation Laboratory Series First Edition, McGraw-Hill Book Company 1948 (TK7803.M3).
2. "A System Approach to Lightweight Modulator Design for Airborne Applications", Major F. S. Zimmerman, et al.
3. O'Loughlin, J.P., Electrical Engineer, Personal Interview, Air Force Weapons Laboratory, Kirtland Air Force Base, New Mexico, December 4, 1980.

APPENDIX A

Mathematical Analysis of DC Resonant Charging

The differential equation for the circuit of Figure 1 is

$$L \frac{d^2q}{dt^2} + R \frac{dq}{dt} + \frac{q}{C} = V(t) \quad (A-1)$$

where q is the instantaneous charge on the network.

The input voltage to the network $V(t)$ was represented as in Equation (1) repeated here for convenience.

$$V(t) = E_{bb} (1 - K i_c(t)) \quad (1)$$

where $i_c(t)$ is the charging current as a function of time, K is a constant and E_{bb} is the peak input voltage.

Figure A-1 shows the plot of Equation (1) for two charging cycles.

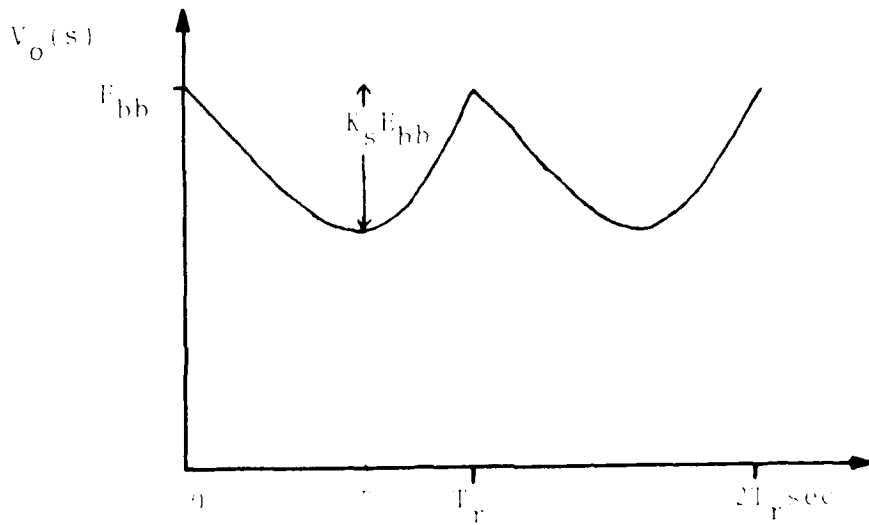


Figure A-1 Plot of Eq(1) for Two Charging Cycles

The constant K is defined by Equation (A-1) below.

$$K = \frac{K_s}{I_{cp}} \quad (A-1)$$

where I_{cp} is the peak value of the charging current. At time $t = 0$, $i_c(0) = I_{cp}$ and equation (1) is then

$$V(t) = E_{bb} (1 - K_s)$$

therefore K_s is the sagging constant and has values from zero to one. For example, if $K_s = 0.1$ the input voltage $V(t)$ has a sagging of 10%, if $K_s = 0.5$ the sagging is 5% and so on.

Substituting $\frac{dq}{dt}$ for $i_c(t)$ and combining Equations (A-1) and (1) we obtain, after rearranging terms,

$$L \frac{d^2q}{dt^2} + (R + \frac{K_s}{I_{cp}} E_{bb}) \frac{dq}{dt} + \frac{q}{C} = E_{bb} \quad (A-3)$$

now let

$$k = \frac{K_s}{I_{cp}} ; b = \frac{R + K_s E_{bb}}{2L} \quad \text{and} \quad w_0^2 = \frac{1}{LC}$$

then Equation (A-3) becomes

$$\frac{d^2q}{dt^2} + 2b \frac{dq}{dt} + w_0^2 q = \frac{1}{L} E_{bb} \quad (A-4)$$

Equation (A-4) is similar to that obtained by Glazee and Lebacqz (Ref. 1; 356-360) the only difference is in the definition of the constant b . The solution for Equation (A-4) are

$$i_c(t) = \frac{E_{bb} - V_0}{WL} e^{-bt} \sin \omega t + I_0 e^{-bt} (\cos \omega t + \frac{b}{\omega} \sin \omega t) \quad (A-5)$$

and

$$V_c(t) = E_{bb} + (E_{bb} - V_0) e^{-bt} (\cos \omega t + \frac{b}{\omega} \sin \omega t) + \frac{I_0}{\omega C} e^{-bt} \sin \omega t \quad (A-6)$$

where

V_0 = Initial capacitor voltage

I_0 = Initial inductor current

$\omega = \sqrt{w_0^2 + b^2}$ = resonance frequency

Equations (A-5) and (A-6) are the expressions for the charging current and capacitor voltage respectively.

Evaluating Equation A-6 at $t = T_r = \frac{\pi}{\omega}$ we find the expression for the voltage in the capacitor at the time of discharge.

$$V_c(T_r) = E_{bb} + [E_{bb} - V_0] e^{-b \frac{\pi}{\omega}} \quad (A-7)$$

The maximum value of Equation (A-5) is found by differentiating the expressions and setting it equal to zero. The initial current I_0 is assumed equal to zero. This is correct because at resonance I_0 is zero and near resonance I_0 is a very small number. The time t at which Equation (A-5) has a maximum value is

$$\phi_{\text{cp}} = \text{ARCTAN} \left(\frac{W}{W} \right)$$

(A-10)

then

$$I_{\text{cp}} = E_{\text{bb}} - \frac{V_0}{W} e^{-bt} \sin \omega t \quad (\text{A-11})$$

In order to evaluate the constant b we need I_{cp} , but I_{cp} is a function of b . The way to solve this is to assume a value of $b = K_s/I_{\text{cp}}$ and evaluate b , then use that value of b with Equations (A-10) and (A-11) to find I_{cp} .

Multiplying the assumed value of b by the computed I_{cp} will give the value of the scaling constant K_s for which this calculation is made.

A small inductance was connected in series with the thyratron tubes to provide an initial negative voltage V_0 . This initial voltage was proportional to the voltage in the capacitor at the discharge time. This factor was called β and was used for calculations in the two computer programs. Substituting $V_0 = \beta V_c(T_r)$ in Equation (A-11) and solving for $V_c(T_r)$ we obtain,

$$V_c(T_r) = E_{\text{bb}} \frac{1 + \text{EXP}(bT_r)}{1 - \beta \cdot \text{EXP}(bT_r)} \quad (\text{A-12})$$

or solving for V_0 ,

$$V_0 = E_{\text{bb}} \frac{1 - \text{EXP}(-bT_r)}{\beta - \text{EXP}(-bT_r)} \quad (\text{A-13})$$

Equations (A-10) and (A-11) were used in the computer programs.

APPENDIX B

Computer Programs

Figure B-1 shows the first of the two computer programs developed to obtain theoretical solutions. This program calculated the resonance frequency, peak capacitor voltage, peak charging current, average current, average voltage, and average power for increasing values of input voltage sag.

The program required as input the value of the circuit components, the peak input voltage E_{bb} , and $P(-V_o/V_c(T_r))$.

The output was the data displayed in Figure 1 through 7 in Chapter II.

Figure B-2 shows the second fortran program. This program calculated the ratio of charging current to average charging current and capacitor voltage to peak input voltage versus time.

The program required as input the value of the circuit components, peak input voltage, $P(-V_o/V_c(T_r))$, constant $K_t = K_s/I_{cp}$, and repetition frequency.

The constant K was found by running the other program first to obtain the set of plots for varying sag constant K_s . The value of peak current for the sag constant of interest was read from the proper curve and K was calculated. If the line where V_o is defined for the second time in the program (see arrow) is changed to $V_o = -PE_{bb} V_{cs}$ the program can be run for repetition frequencies higher than resonance.

Figure B-1 Fortran Program for Varying Sag Constant

Figure B-2a Fortran Program for Charging Current and Capacitor Voltage Waveforms (Sheet 1 of 2)

Figure B-2b Fortran Program for Charging Current and Capacitor Voltage Waveforms (Sheet 2 of 2)

This program runs for more than one cycle by storing the final value of the current as the initial value for the next cycle and resetting the voltage in the capacitor to a negative value proportional to the voltage at the time of discharge.

The output of this program was the data displayed in Figure 8 through 12 in Chapter II.

APPENDIX C

Additional Case

Figure (C-1) shows the DC bus voltage and the charging current for 15KW output power of the generator.

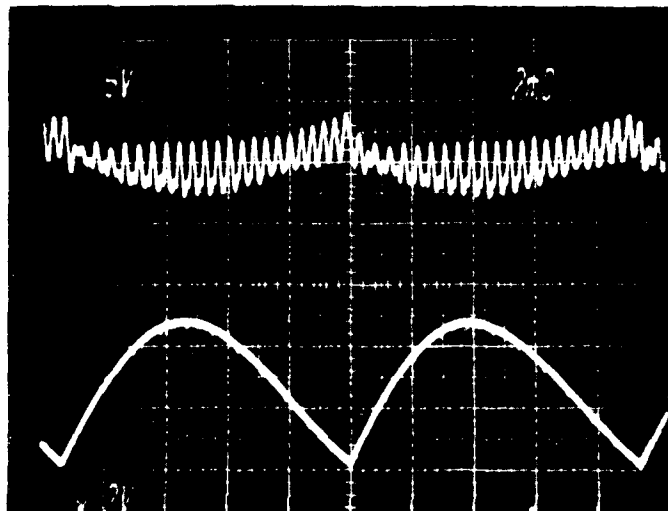


Figure C-1 Scope Trace of DC Bus Voltage (10P) and Charging Current (5KV/div, 2A/div)

From visual inspection of Figure C-1 the following values are obtained:

$$I_{bb} \approx 8\text{KV}$$

$$K_s \approx 0.50$$

$$I_{cp} \approx 1.6 \text{ AMP}$$

the resonance frequency was 106.6Hz and $\mu = 0.055$. The computer calculated value of $V_c(t_r)$ was 10.3 KV. Figure (C-2) shows the DC bus voltage and the capacitor voltage for this case. The actual value of the peak capacitor voltage was 9.6KV.

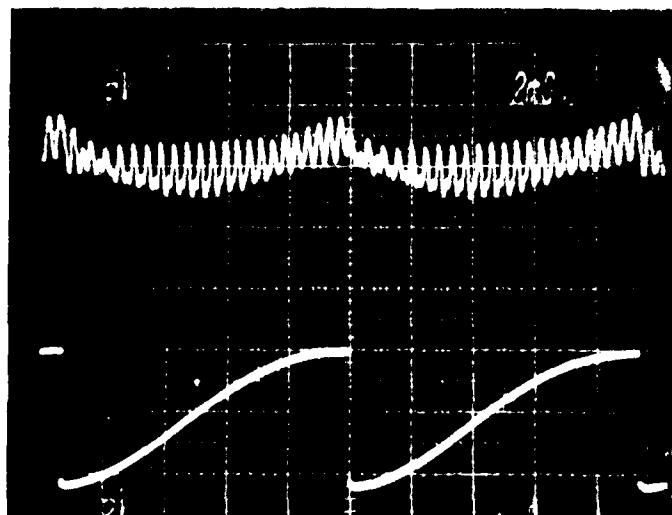


Figure C-2 Scope Trace of DC Bus Voltage (10V) and Capacitor Voltage (5kV/div)

The theoretical peak charging current was 5.0 A/P, the average power 17kW, and the resonance frequency 108.5Hz.

APPENDIX D
Major Parts List

General

DYNAMO - GE 150 HP dynamometer

GENERATOR - 15 KW DOD Standard

400 Hz, 210 V, 26A, 2000 RPM

THYRATRONS - JAN 8615, 5Mr Peak Power,

20KV Peak ANODE Voltage, 5mA

Peak Forward Current

DC Resonant

Transformer - 50KV, 400 Hz, 416:100W

Rectifiers - liquid cooled test inhouse

Rectifier assembly, 64 KV, PVA, 50 AMP nominal current

AC Resonant

Transformers - Three 400 Hz Transformers, 240:440V,
4.5 AMO secondary nominal current, 64.44-62.82-64.23 pu
leakage reactance and 4.25-4.20-4.17 pu resistance respe-
tively.

Charging Diodes - rectifier stack with 50FA PEL, 10KV
nominal current.

Vita

Jaime Roberto Silva was born on 11 October 1956 in San Juan, Puerto Rico. He graduated from high school in Rio Piedras, Puerto Rico in 1974 and attended the University of Puerto Rico Mayaguez campus from which he received the degree of Bachelor of Science in Electrical Engineering in June 1979. Upon graduation he received a commission in the United States Air Force through the ROTC program and entered the School of Engineering, Air Force Institute of Technology in June 1979.

Permanent Address: 327 Barnard Street
Rio Piedras, Puerto Rico 00926

SECURITY CLASSIFICATION OF THIS PAGE WHEN DRAFTED.

| REPORT DOCUMENTATION PAGE | | READ INSTRUCTIONS BEFORE COMPLETING FORM |
|--|--------------------------|---|
| 1. REPORT NUMBER | 2. GOV'T ACQUISITION NO. | 3. REPORTING ORGANIZATION NUMBER |
| DL Alice 827 | | |
| 4. TITLE (Include subtitle if applicable) | | |
| 5. CONTRACT NUMBER | | |
| 6. DATA SOURCE | | |
| 7. DATE OF REPORT | | |
| 8. APPROXIMATE NUMBER OF PAGES | | |
| 9. APPROXIMATE NUMBER OF FIGURES | | |
| 10. APPROXIMATE NUMBER OF TABLES | | |
| 11. APPROXIMATE NUMBER OF APPENDICES | | |
| 12. APPROXIMATE NUMBER OF REFERENCES | | |
| 13. APPROXIMATE NUMBER OF PICTURES | | |
| 14. APPROXIMATE NUMBER OF DRAWINGS | | |
| 15. APPROXIMATE NUMBER OF PLATES | | |
| 16. APPROXIMATE NUMBER OF CHARTS | | |
| 17. APPROXIMATE NUMBER OF TABLETS | | |
| 18. APPROXIMATE NUMBER OF COMPUTER PROGRAMS | | |
| 19. APPROXIMATE NUMBER OF COMPUTER PROGRAMS | | |
| 20. ABSTRACT | | |
| A. ABSTRACT (Type or print abstract on a separate sheet of paper and identify by block number) B. KEY WORDS (Type or print key words on a separate sheet of paper and identify by block number) C. APPROXIMATE NUMBER OF PAGES | | |
| D. APPROXIMATE NUMBER OF FIGURES | | |
| E. APPROXIMATE NUMBER OF TABLES | | |
| F. APPROXIMATE NUMBER OF APPENDICES | | |
| G. APPROXIMATE NUMBER OF REFERENCES | | |
| H. APPROXIMATE NUMBER OF PICTURES | | |
| I. APPROXIMATE NUMBER OF DRAWINGS | | |
| J. APPROXIMATE NUMBER OF PLATES | | |
| K. APPROXIMATE NUMBER OF CHARTS | | |
| L. APPROXIMATE NUMBER OF TABLETS | | |
| M. APPROXIMATE NUMBER OF COMPUTER PROGRAMS | | |
| N. APPROXIMATE NUMBER OF COMPUTER PROGRAMS | | |
| O. APPROXIMATE NUMBER OF COMPUTER PROGRAMS | | |
| P. APPROXIMATE NUMBER OF COMPUTER PROGRAMS | | |
| Q. APPROXIMATE NUMBER OF COMPUTER PROGRAMS | | |
| R. APPROXIMATE NUMBER OF COMPUTER PROGRAMS | | |
| S. APPROXIMATE NUMBER OF COMPUTER PROGRAMS | | |
| T. APPROXIMATE NUMBER OF COMPUTER PROGRAMS | | |
| U. APPROXIMATE NUMBER OF COMPUTER PROGRAMS | | |
| V. APPROXIMATE NUMBER OF COMPUTER PROGRAMS | | |
| W. APPROXIMATE NUMBER OF COMPUTER PROGRAMS | | |
| X. APPROXIMATE NUMBER OF COMPUTER PROGRAMS | | |
| Y. APPROXIMATE NUMBER OF COMPUTER PROGRAMS | | |
| Z. APPROXIMATE NUMBER OF COMPUTER PROGRAMS | | |

SECURITY CLASSIFICATION OF THIS PAGE When Data Entered

